Physics

SCIENCE OF LIGHT

VOLUME 2 NUMBER 2

March
1953

Published by the

Institute for Optical Research
Tokyo University of Education

SCIENCE OF LIGHT

Science of Light contains reports of the Institute for Optical Research and contributions from other science bodies about similar subject.

All communications should be addressed to the director or to the librarian of the Institute.

The Institute for Optical Research

Tokyo University of Education

400, 4-chome, Hyakunin-machi, Sinjuku-ku, Tokyo, Japan

Printed by SANYOSHA PRITING Co., TOKYO

On the Absorption Spectrum in the $1s\sigma 3p\pi\,{}^1\Pi_{cd}$–$(1s\sigma)^2\,{}^1\Sigma_g^+$ System of the Hydrogen Molecule

Takeshi NAMIOKA

Institute for Optical Research, Tokyo University of Education

(Received Oct. 15, 1952)

The absorption spectrum of the hydrogen molecule in the extreme ultraviolet region 900 to 700 Å was photographed by the use of a 3-meter grazing incidence vacuum spectrograph. Helium continuum was employed as light source for the continuous background.

In treating the D–A band system that has not yet been completely analysed up to now, the writer has been successful in analysing nine bands from (0–0) to (8–0) and in deriving various molecular constants of each state.

The molecular constants for the $1s\sigma 3p\pi\,{}^1\Pi_{cd}$ are expressed by

$$(B_v^x)_c = 30.519 - 1.5156\left(v+\frac{1}{2}\right) - 0.0057699\left(v+\frac{1}{2}\right)^2 + 0.0015170\left(v+\frac{1}{2}\right)^3,$$

$$(B_v^x)_d = 31.942 - 1.6353\left(v+\frac{1}{2}\right) - 0.03009\left(v+\frac{1}{2}\right)^2 - 0.00096597\left(v+\frac{1}{2}\right)^3,$$

$$(D_v^x)_c = -0.02371 - 0.00207\left(v+\frac{1}{2}\right) + 0.0001131\left(v+\frac{1}{2}\right)^2,$$

$$(D_v^x)_d = -0.02604 + 0.0009863\left(v+\frac{1}{2}\right) - 0.00001673\left(v+\frac{1}{2}\right)^2.$$

These values are slightly different from those of Jeppesen and Tanaka who used the data of vibrational states.

1 Introduction

The absorption spectrum of the hydrogen molecule was first investigated by Hopfield[1), 2)] in 1930. He found, in addition to the B—A and C—A band systems, another band system consisting of eight bands further in the extreme ultraviolet region between 838 anb 771 Å. These bands were degraded towards the red, and the (0—0) band of this system was 838.62 Å. According to Hopfield the electronic levels concerned were a normal and a new D levels 14.7 volts above the former. He further pointed out that the formula representing these band heads was $\nu = 119244 + 1900v' - 59.24v'^2$, that the energy of dissociation from the D state was 1.872 volts, and that the products of dissociation of this state were a normal hydrogen atom and another excited to the 3-quantum state.

In 1933 Richardson[3)] pointed out a fault in Hopfield's quantum assignment

1) J. J. Hopfield: Phys. Rev., **35** (1930) 1133; 2) J. J. Hopfield: Nature, **125** (1930) 927;
3) O. W. Richardson: *Molecular Hydrogen and Its Spectrum*, (1933) 97~98, 303~305.

for this band progression and concluded that the true assignment of the observed absorption bands should be $v'=3, 4, 5, \cdots\cdots, 10$, because the amount of the predicted dissociation energy of this state, and that of the vibrational quanta ω_0 were more reasonable than the one derived from the Hopfield's assignment. The reason why he thought that the bands with $v'=0, 1, 2$ had been overlooked was partly because they were covered by an intense continuous absorption in the same region and partly because they were mixed with the bands of higher vibrational levels of the C—A band.

In 1935 Hopfield[4] again photographed the H_2 absorption spectrum in the region above mentiomed and observed discrete absorption lines belonging to the D—A band system and also a new system extending into the region above the ionization potential of H_2 (15.9 eV), but he did not publish any numerical data in his paper. In conclusion he stated that no new vibration bands of this system were evident to change the vibrational analysis that had already been given by Hopfield.

In 1936 Beutler, Deubner and Jünger[5] photographed the absorption spectrum of H_2 and D_2 in the region 900 to 600 Å by the use of the first and second orders of a 1-meter concave grating. By means of the vibrational isotope shift, they showed that the absorption band progression began with the $v'=3$ level of the D state, thus endorsing Richardson's alternative quantum assignment. They obtained the following formula for each band:

$$\nu_0 = 111849 + 2315\left(v' + \frac{1}{2}\right) - 59.25\left(v' + \frac{1}{2}\right)^2, \quad v' = 3, 4, 5, \cdots\cdots, 10.$$

Furthermore they predicted the possibility of the predissociation of these bands, because these levels of the D state lay energetically above the chemical dissociation limit and showed a strong diffuse character.

In the same year, Beutler and Jünger[6] found a remarkably diffuse character; the $R(2)$, $R(3)$, $R(4)$, $P(4)$ and $P(5)$ lines of the (6—0) band being diffuse in a striking contrast to the sharp $R(0)$, $R(1)$, $P(2)$, $P(3)$ and Q branch lines. They attributed this diffuseness to such autoionization as $H_2^* = H_2^+$

4) J. J. Hopfield: Phys. Rev., **47** (1935) 788; 5) H. Beutler, A. Deubner and H. O. Jünger: Zeits. f. Phys., **100** (1936) 181; 6) H. Beutler and H. O. Jünger: Zeits. f. Phys., **100** (1936) 80;

$+e_u$, partly because the rotational energy of the $v'=6$ level of the D state is energetically equal to that of the $v'=0$ of the ground state $1\sigma^1\Sigma_g^+$ of H_2^+ and partly because these two states very nearly satisfied Kronig's selection rule[7]. However, their analysis covered only the (6—0) and not all the bands. Moreover they asserted that the abnormal intensity of the (3—0) band might be attributable to a predissociation due to the crossing of an unstable state which would bring about dissociation into two atoms, one normal and the other excited to the 2-quantum state. But no mention was made in their paper of the missing bands ($v'<3$) discussed above.

In 1938 Jeppesen[8] succeeded in observing the D-A band system of H_2 in the emission spectrum by using a vacuum spectrograph containing a 2-meter concave grating. He derived the vibrational and rotational constants through the analysis of the ten bands related to the transition from the first three vibrational levels of the D state to the ground state. As none of the emission bands he obtained were on vibrational levels higher than the third, he attributed this fact to the existence of a predissociation at $v'=3$ in the D state. And then as a result of rotational analysis he also found a perturbation existing between $v'=9$ of the C state and $v'=1$ of the D state.

More recently the missing bands mentioned above were observed for the first by Tanaka[9] in his absorption spectrum of H_2. The experiment was undertaken on the assumption that if the two difficulties pointed out by Richardson were eliminated the missing bands could have been obtained together with the bands of $v'<3$, because the predissociation seemed to fall on case I(c) as classified by Herzberg[10]. The missing bands were actually analysed, and the existence of a predissociation were also verified.

As above mentioned, though the D-A band system has been partially analysed by many investigators, a complete rotational analysis has never yet been performed until now, and this induced the writer to photograph the absorption D-A band spectrum with the view of performing a complete rotational analysis.

2 Experiment

The experimental arrangments were exactly the same as reported in

7) R. de L. Kronig: Zeits. f. Phys., **46** (1927) 814 and **50** (1928) 347; 8) C. R. Jeppesen: Phys. Rev., **54** (1938) 68; 9) Y. Tanaka: Sci. Pap. I. P. C. R., **42** (1944) 49; 10) G. Herzberg: *Ergebnisse der exakten Naturwissenshaften X*, (1931) 241.

Tanaka's paper[11] on the absorption on nitrogen except that hydrogen was used instead of the former gas. A 3-meter grazing incidence type vacuum spectrograph was used and helium continuum was employed as the light source for the background.

The pressure of hydrogen in the spectrograph tank was kept at 0.001 mmHg throughout the experiment, and since the existence of water vapor as impurity in the hydrogen would be very detrimental the gas was prepared in the following manner hydrogen obtained by electrolysis of a distilled solution of KOH was stored one whole day in a flask containing P_2O_5 and then introduced into the spectrograph through a trap immersed in liquid air. The photographic plates employed here were so-called Schuman plates, and the time of exposure 40 to 70 minutes. The errors in the measurement of wavelength were not likely to exceed 0.15 Å for diffuse lines and 0.03 Å for sharp lines.

3 Result

The important aim of the present investigation was to analyse the D-A band system as completely as possible. Typical photographic plates are shown in Pl. 1.

In the region to be discussed no conspicuous continuous absorption spectrum as suggested by Richardson were found, but this stretch was filled with so many absorption lines that it made identification difficult. Fortunately, however, the intensity of each $v' \geqq 3$ band head was very strong compared with other lines, and apparent doublet lines existing at their heads together with the increasing separation and sharpness with progressing v' provided helpful aids for the analysis. The vibrational quantum assignment was therefore made with the use of the character of the doublet of each band head and by searching around the position of the calculated wavelength.

In the present investigation the positions of the rotational lines of the $v' \leqq 2$ bands were tentatively calculated by the use of Tanaka's molecular constants, and then the positions of the $v' \geqq 3$ bands calculated by using the constants already obtained for all the preceding bands. Moreover each line was accurately identified by the use of the following combination relation:

$$R(K+1)-P(K)=\Delta_2 F'_d(K), \qquad (1)$$

11) Y.Tanaka: Sci. Pap. I. P .C. R., 39 (1942) 427.

$$Q(K+1)-Q(K)+F''(K+1)-F''(K)=\Delta F'_c\left(K+\frac{1}{2}\right). \qquad (2)$$

All the rotational lines identified in the present investigation are summarized in Table 1.

(A) The rotational analysis

The Rotational energy function for a $^1\Pi$ state was given by Mulliken[12), 13)] as follows:

$$F_v(K)=B_v\left[\left(K+\frac{1}{2}\right)^2-\Lambda^2+G^2\right]+\varphi_i(K)+D_v\left[\left(K+\frac{1}{2}\right)^4+\cdots\cdots\right]$$
$$+H_v\left[\left(K+\frac{1}{2}\right)^6+\cdots\cdots\right], \qquad (3)$$

in which uncoupling term $\varphi_i(K)$ is given by [13)]

$$\varphi_i(K)=\kappa_i+\delta_i\left(K+\frac{1}{2}\right)^2+\mu_i\left(K+\frac{1}{2}\right)^4+\cdots\cdots, \qquad (4)$$

where $\delta_i \gg \mu_i \gg \cdots\cdots$, and κ_i is of the same order of magnitude as δ_i. By putting

$$B_i^x=B_v+\delta_i\,, \qquad D_i^x=D_v+\mu_i\,,\cdots\cdots \qquad (5)$$

$\varphi_i(K)$ in eq. (4) may be combined with the other terms in eq. (3). Since the

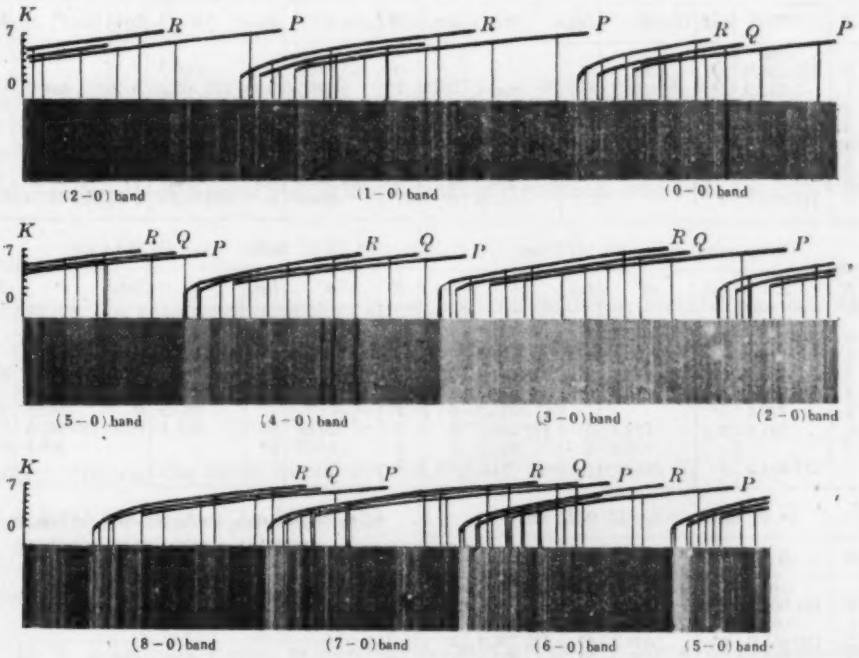

PL. 1 Absorption spectrum of D-A band system.

12) R. S. Mulliken: Rev. Mod. Phys., **2** (1930) 100; 13) R. S. Mulliken: Rev. Mod. Phys., **3** (1931) 102.

Table 1.

The analysed data of the D←A bands.

(0-0) band $\nu_0 = 112\,891.0$ cm^{-1}

K	R	Int.	Q	Int.	P	Int.
	cm^{-1}					
0	112 944.8	2*	cm^{-1}			
1	944.8	2*	112 824.6	0.5	cm^{-1}	
2	897.8	2	707.3	0.5	112 589.8	2
3	784.9	1.5	532.3	1.5	357.0	0.5
4	624.3	0.5	299.8	0.5	083.0	0.5
5	404.9	2	015.4	0	111 750.5	0
6	158.9	0.5			400.5	0.5

(1-0) band $\nu_0 = 115\,111.0$ cm^{-1}

K	R	Int.	Q	Int.	P	Int.
	cm^{-1}					
0	115 156.5	2*	cm^{-1}			
1	156.5	2*	115 041.1	2	cm^{-1}	
2	093.3	0	114 917.4	0.5	114 806.2	0.5
3	114 955.6	0.5	732.6	0.5	565.6	0
4			437.8	0	277.1	0.5
5	523.2	0	186.2	0	113 923.4	0.5
6					521.6	0
7	113 849.5	0			069.2	0

(2-0) band $\nu_0 = 117\,205.1$ cm^{-1}

K	R	Int.	Q	Int.	P	Int.
	cm^{-1}					
0	117 250.0	2*	cm^{-1}			
1	243.9	2*	117 131.7	0.5	cm^{-1}	
2	171.5	0.5	001.6	0	116 893.0	0.5
3	036.8	0.5	116 807.5	0	656.1	0.5
4			550.5	0		
5	116 569.5	0	232.2	0	115 996.9	0
6					594.9	0
7	115 878.2	0			107.0	0

(3-0) band $\nu_0 = 119\,187.5$ cm^{-1}

K	R	Int.	Q	Int.	P	Int.
	cm^{-1}					
0	119 226.2	6*	cm^{-1}			
1	216.1	6*	119 109.2	6	cm^{-1}	
2	135.0	6*	118 973.4	3	118 871.3	0.5
3	118 994.1	3	770.6	0*	628.7	0.5
4	770.6	0*			310.7	0
5	521.0	0	172.3	0	117 962.7	0
6			776.0	0	551.2	0
7	117 814.5	0			081.5	0.5

(4-0) band $\nu_0 = 121\,022.3$ cm^{-1}

K	R	Int.	Q	Int.	P	Int.
	cm^{-1}					
0	121 062.4	7*	cm^{-1}			
1	047.5	7*	120 942.4	7*	cm^{-1}	
2	120 955.0	7*	800.7	3*	120 706.2	2
3	800.7	3*	589.0	0*	455.3	0
4	589.0	0*	308.4	2*	151.6	0
5	308.4	2*			119 781.6	0
6	119 976.2	0	119 539.9	0	364.5	0
7						

(5-0) band $\nu_0 = 122\,767.5$ cm^{-1}

K	R	Int.	Q	Int.	P	Int.
	cm^{-1}					
0	122 772.8	5	cm^{-1}			
1	745.2	5	122 630.9	3	cm^{-1}	
2	651.8	0	532.9	3	122 417.7	3
3	482.2	0			157.8	3
4	243.7	0			121 832.0	0.5
5	121 947.9	0	121 656.5	0	452.6	0
6	589.4	0	224.7	0	017.8	7*

(6-0) band $\nu_0 = 124\,368.5$ cm^{-1}

K	R	Int.	Q	Int.	P	Int.
	cm^{-1}					
0	124 390.3	5	cm^{-1}			
1	355.2	5	124 281.7	0	cm^{-1}	
2	255.0	0	127.8	0.5	124 033.9	2
3	081.2	3	123 897.8	0.5	123 776.6	2
4	193 823.0	0	592.5	0	442.9	0
5					054.9	0
6	137.6	0			122 596.5	0
7						

(7-0) band $\nu_0 = 125\,853.1$ cm^{-1}

K	R	Int.	Q	Int.	P	Int.
	cm^{-1}					
0	125 876.1	5	cm^{-1}			
1	840.5	5	125 762.9	3	cm^{-1}	
2	727.9	3	603.9	0	125 521.1	0.5
3	534.8	0.5	366.2	0	248.3	0
4	267.3	0				
5			124 659.3	0	124 497.7	2
6	124 542.4	0.5	193.5	3	035.9	2
7	054.9	0	123 649.5	0	123 482.4	0

(8-0) band $\nu_0 = 127\,218.4$ cm^{-1}

K	R	Int.	Q	Int.	P	Int.
	cm^{-1}					
0	127 237.7	5*	cm^{-1}			
1	200.7	5*	127 128.9	5	cm^{-1}	
2	067.2	5*			126 873.3	2*
3	126 873.3	2*	126 714.0	0		
4			387.5	0	249.6	0*
5	249.6	0*	981.4	0.5	125 840.5	5*
6	840.5	5*			366.2	0*
7						

Note: Symbole * indicates that its line is overlapping with other rotational line.

term $B_v(\bar{G}^2-\Lambda^2)$ is too small to be separated from the electronic energy, if the values of eq. (4) and eq. (5) are substituted into the right hand of eq. (3), eq. (3) may be expressed in the following convenient form·

$$F_v(K)= {}^xB_i\left(K+\frac{1}{2}\right)^2+D_i^x\left(K+\frac{1}{2}\right)^4+H_i^x\left(K+\frac{1}{2}\right)^6+\cdots\cdots, \qquad (6)$$

where B_i^x, D_i^x, H_i^x and so on are so-called effective values, the lower subscript i denoting the c and d component levels in the Λ type doubling, and the upper subscript x used to signify "*ffective*".

The Λ type doubling was discussed by Hund[14] and later by Kronig[15], Hill and van Vleck[16], and still later treated in full detail by Mulliken[17]. Van Vleck[18] has shown that the $^1\Pi_{cd}$ state possesses the following double forms:

$$\varphi_c(K)=-2C+\left(C+C_2\right)\left(K+\frac{1}{2}\right)^2, \qquad (7)$$

and

$$\varphi_d(K)=-2C+\left(C+C_1\right)\left(K+\frac{1}{2}\right)^2. \qquad (8)$$

According to Hill and van Vleck, $C=0$ and $C_2=0$ in the present case. Hence, by letting $C=0$ and $C_2=0$ in eq. (7) and (8), we may easily obtain the formula for $\varphi_i(K)$ as follows: $\varphi_c(K)=0$ and $\varphi_d(K)=C_1\left(K+\frac{1}{2}\right)^2$.

Therefore, in this case $(B_v^x)_c$ gives the true B_v values that determine the value of the moment of inertia and other molecular constants, and $(B_v^x)_d$ is expressed by

$$(B_v^x)_d=B_v+C_1.$$

To derive the rotational molecular constants, the following method was adopted:

For the d component level the well known relation

$$R(K)-P(K)=\Delta_2F'_d(K)$$

is used, and on the other hand, since $\Delta_2F'_d(K)$ is expressed by

$$\Delta_2F'_d(K)=F'_d(K+1)-F'_d(K-1)$$

$$=\left(K+\frac{1}{2}\right)\left[4(B_v^x)_d+8(D_v^x)_d\left\{\left(K+\frac{1}{2}\right)^2+1\right\}+(H_v^x)_d\left\{12\left(K+\frac{1}{2}\right)^4\right.\right.$$

14) F. Fund: Zeits. f. Phys., **36** (1926) 657 and **42** (1927) 93; 15) R. de L. Kronig: Zeits. f. Phys., **46** (1928) 814 and **50** (1928) 347; 16) E. L. Hill and J. H. van Vleck: Phys. Rev., **32** (1928) 250; 17) R. S. Mulliken: Phys. Rev., **33** (1929) 507; 18) J. H. van Vleck: Phys. Rev., **33** (1929) 467.

$$+40\left(K+\frac{1}{2}\right)^2+12\Big\}\Big],$$

we used the equation

$$\frac{R(K)-P(K)}{K+\frac{1}{2}}=4(B_v^x)_d+8(D_v^x)_d\left\{\left(K+\frac{1}{2}\right)^2+1\right\}+(H_v^x)_d\left\{12\left(K+\frac{1}{2}\right)^4\right.$$

$$\left.+40\left(K+\frac{1}{2}\right)^2+12\right\} \qquad (9)$$

for the calculation of $(B_v^x)_d$, $(D_v^x)_d$ and $(H_v^x)_d$. By substituting the numerical values of $\Delta_2F'_d(K)$ in Table 1 into the left hand of eq. (9) and by using the method of least squares, the most probable values $(B_v^x)_d$, $(D_v^x)_d$ and $(H_v^x)_d$ can be obtained. Here, since the variation of the value of $(H_v^x)_d$ with v' is expected to be neglegibly small, in the present investigation the value of $(H_o^x)_d$ obtained through the analysis of the (0-0) band is used to represent those of $(H_v^x)_d$ and $(H_e^x)_d$.

The numerical values of $\Delta_2F'_d(K)$ and of $(B_v^x)_d$, $(D_v^x)_d$ are shown in Tables 2 and 3, respectively.

Table 2

The numerical values of $\Delta_2F'_d(K)$

v' \ K	2	3	4	5	6	7
0	308.0 cm^{-1}	427.9 cm^{-1}	541.3 cm^{-1}	654.4 cm^{-1}	758.4 cm^{-1}	
1	287.1	390.0		599.8		780.3 cm^{-1}
2	278.5	380.7		572.6		772.2
3	263.7	365.4	461.9	558.3		733.0
4	248.8	345.4	437.4	526.8	611.7	
5	234.1	324.4	411.7	495.3	571.6	
6	221.1	304.6	380.1		541.1	
7	206.8	286.5			506.5	572.5
8	193.9			409.1	474.3	

Table 3

The numerical values of $(B_v^x)_d$ and $(D_v^x)_d$

v'	0	1	2	3	4	5	6	7	8
$(B_v^x)_d$	cm^{-1} 31.165	cm^{-1} 28.736	cm^{-1} 27.862	cm^{-1} 26.652	cm^{-1} 25.193	cm^{-1} 23.703	cm^{-1} 22.230	cm^{-1} 20.952	cm^{-1} 19.651
$(D_v^x)_d$	−0.02508	−0.02660	−0.02331	−0.02230	−0.02148	−0.02068	−0.01988	−0.01913	−0.01843

As to the c component level, we unfortunately can not calculate it in such simple a manner as in the case of the d component level. In the present case the values of the rotational energy in the ground state of H_2 must be newly introduced into the calculation. For this we adopted the numerical values of Jeppesen as the values of the rotational energy in the ground state of H_2.

For the c component level, the following method was adopted for the derivation of the molecular constants:

For the familiar relation $$Q(K)=\nu_0+F'_c(K)-F''(K) \tag{10}$$

we have: $$Q(K+1)-Q(K)=F'_c(K+1)-F'_c(K)+F''(K)-F''(K+1), \tag{11}$$

and since by difinition $$F(K+1)-F(K)=F\left(K+\frac{1}{2}\right) \tag{12}$$

we immediately obtain from eq. (11):

$$\Delta F'_c\left(K+\frac{1}{2}\right)=Q(K+1)-Q(K)+\Delta F''\left(K+\frac{1}{2}\right). \tag{13}$$

On the other hand $\Delta F'_c\left(K+\frac{1}{2}\right)$ is expressed by the following formula:

$$\Delta F'_c\left(K+\frac{1}{2}\right)=(K+1)\left[2(B_v^x)_c+(D_v^x)_c\left\{4(K+1)^2+1\right\}\right.$$
$$\left.+(H_v^x)_c\left\{6(K+1)^4+5(K+1)^2+\frac{3}{8}\right\}\right]. \tag{14}$$

Therefore, the value of $\left\{Q(K+1)-Q(K)+\Delta F''\left(K+\frac{1}{2}\right)\right\}\Big/(K+1)$ is given by,

$$\left\{Q(K+1)-Q(K)+\Delta F''\left(K+\frac{1}{2}\right)\right\}\Big/(K+1)=2(B_v^x)_c+(D_v^x)_c\left\{4(K+1)^2+1\right\}$$
$$+(H_v^x)_c\left\{6(K+1)^4+5(K+1)^2+\frac{3}{8}\right\}. \tag{15}$$

As the difference of the values of H_v^x in the c and d component levels was expected to be very small in the present study, the value of $(H_0^x)_d$ was used as that of $(H_v^x)_c$, and Jeppesen's values were employed as the $\Delta F''\left(K+\frac{1}{2}\right)$ for this calculation. With these the $(B_v^x)_c$ and $(D_v^x)_c$ values can be calculated from the following equation:

$$\frac{1}{K+1}\left\{Q(K+1)-Q(K)+\Delta F''\left(K+\frac{1}{2}\right)\right\}-(H_0^x)_d\left\{6(K+1)^4+5(K+1)^2+\frac{3}{8}\right\}$$

$$=2(B_v^x)_c+(D_v^x)_c\{4(K+1)^3+1\}. \quad (16)$$

The values of the rotational energy of the ground state obtained by Jeppesen are shown in Table 4. The values of the left hand of eq. (16) are shown in Table 5.

Table 4.

The numerical values of the rotational energy of the ground state obtained by C. R. Ieppesen.

K	$F''(K)$	$F''(K+1)-F''(K)$
0	14.84 cm^{-1}	118.47 cm^{-1}
1	133.31	235.88
2	369.19	351.11
3	720.30	463.25
4	1183.55	571.39
5	1754.94	672.83
6	2427.77	775.05
7	3202.82	

Table 5

The numerical values of $\Delta F'_c\left(K+\frac{1}{2}\right)$

K / v	1	2	3	4	5	6
0	118.58 cm^{-1}	176.11 cm^{-1}	230.75 cm^{-1}	286.99 cm^{-1}		
1	112.18	166.31	218.45	269.79		
2	105.78	157.01	206.25	253.09		
3	100.08	148.31			276.53 cm^{-1}	
4	94.18	139.41	182.65			
5	87.88				241.03	
6	81.98	121.11	157.95			
7	76.88	113.41			207.03	
8			136.75	165.29		231.05 cm^{-1}

Now by putting the numerical values of Table 5 in the left hand of eq. (16) and by means of the least square method, the values of $(B_v^x)_c$ and $(D_v^x)_c$ are determined as shown in Table 6.

Table 6.

The numerical values of $(B_v^x)_c$ and $(D_v^x)_c$

v'	0	1	2	3	4	5	6	7	8
$(B_v^x)_c$	cm^{-1} 29.775	cm^{-1} 28.225	cm^{-1} 26.685	cm^{-1} 25.202	cm^{-1} 23.800	cm^{-1} 22.259	cm^{-1} 20.767	cm^{-1} 19.498	cm^{-1} 18.153
$(D_v^x)_c$	−0.02434	−0.02682	−0.02851	−0.02972	−0.03068	−0.03138	−0.03220	−0.03276	−0.03339

By the use of the numerical values of Tables 3 and 6, the least square equations of $(B_v^x)_{c,d}$ and $(D_v^x)_{c,d}$ are expressed as follows:

$$(B_v^x)_c = 30.519 - 1.5156\left(v+\frac{1}{2}\right) - 0.0057699\left(v+\frac{1}{2}\right)^2 + 0.0015170\left(v+\frac{1}{2}\right)^3, \quad (17)$$

$$(B_v^x)_d = 31.942 - 1.6353\left(v+\frac{1}{2}\right) - 0.0309\left(v+\frac{1}{2}\right)^2 - 0.00096597\left(v+\frac{1}{2}\right)^3, \quad (18)$$

$$(D_v^x)_c = -0.02371 - 0.00207\left(v+\frac{1}{2}\right) + 0.0001131\left(v+\frac{1}{2}\right)^2, \quad (19)$$

$$(D_v^x)_d = -0.02604 + 0.0009863\left(v+\frac{1}{2}\right) - 0.00001673\left(v+\frac{1}{2}\right)^2 \quad (20)$$

$(B_v^x)_{c,d}$: v curves and $(D_v^x)_{c,d}$: v curves are shown in Figs. 1 and 2.

The moment of inertia and the internuclear distance are calculated as shown in Table 9.

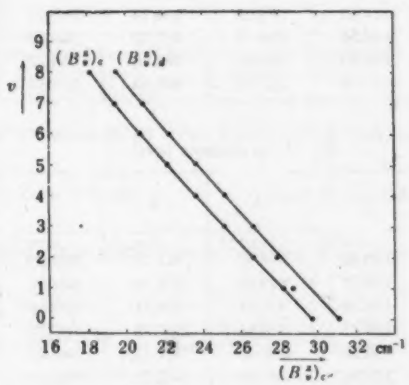

Fig. 1 $(B_v^x)_{cd}$: v for the D state

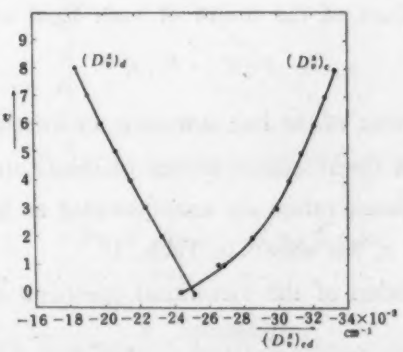

Fig. 2 $(D_v^x)_{cd}$: v for the D state.

(B) The vibrational analysis

By using the rotational constants obtained by the rotational analysis in the previous paragraph (A) the values of the rotational energy of the D state can be calculated from eq. (3). The values of the rotational energy obtained are listed in Table 7.

Table 7

The values of the rotational energy of the D state.

(1) ϵ component level.

v \ K	0	1	2	3	4	5	6	7
	cm^{-1}	cm^{-1}	cm^{-1}	cm^{-1}	cm^{-1}	cm^{-1}	cm^{-1}	cm^{-1}
0	7.44	66.87	185.15	361.15	593.23	879.31	1216.96	1603.53
1	7.05	63.37	175.37	341.79	560.82	830.15	1147.04	1508.49
2	6.67	59.90	165.68	322.67	528.95	782.02	1078.96	1416.52
3	6.30	56.55	156.36	304.32	498.42	736.05	1014.15	1329.27
4	5.95	53.40	147.56	287.00	469.64	692.76	953.20	1247.37
5	5.56	49.92	127.90	268.02	438.14	645.51	886.84	1158.43
6	5.19	46.56	128.54	249.52	407.59	599.62	822.34	1017.95
7	4.87	43.70	120.59	223.99	381.66	560.72	767.72	993.80
8	4.52	40.67	112.15	217.36	353.90	518.57	707.36	915.56

(2) d component level

v \ K	0	1	2	3	4	5	6	7
	cm^{-1}	cm^{-1}	cm^{-1}	cm^{-1}	cm^{-1}	cm^{-1}	cm^{-1}	cm^{-1}
0	7.79	69.99	193.81	378.07	621.07	920.68	1274.36	1679.37
1	7.18	64.52	178.57	348.08	571.26	845.81	1169.02	1537.93
2	6.96	62.57	173.23	337.87	554.91	822.38	1137.97	1499.18
3	6.66	59.85	165.71	323.18	530.82	786.70	1088.65	1434.31
4	6.29	56.57	156.62	305.45	501.61	743.32	1023.47	1354.84
5	5.92	53.23	147.34	287.32	471.77	698.93	966.95	1273.55
6	5.55	49.92	138.17	269.39	452.27	655.15	906.14	1193.23
7	5.23	47.04	130.21	253.85	416.70	617.18	853.49	1123.71
8	4.91	44.12	122.10	238.02	390.64	578.55	799.77	1052.75

Then, the numerical values of the origin of each band are obtained from the familiar relation

$$\nu_0=\nu-F'(K')+F''(K'') \tag{21}$$

where ν is the wave number of the line belonging to a certain band, and $F'(K')$ and $F''(K'')$ the values of the rotational energy of the D and ground states, respectively. Here, the Jeppesen values are again adopted as the values of $F''(K'')$. The numerical values of ν_0 are shown in Table. 1.

Now, in the calculation of the vibrational constants of this state we used the well known formula

$$\Delta G_{v+\frac{1}{2}}=G(v+1)-G(v)=\nu_0^{(v+1,\,0)}-\nu_0^{(v,\,0)}=\omega_e-2\omega_e x_e-2\omega_e x_e v+\cdots\cdots. \tag{22}$$

Replacing $v+\frac{1}{2}$ by V, we obtain the following convenient formula:

$$\Delta G_V=\omega_e-2\omega_e x_e\left(V+\frac{1}{2}\right)+\cdots\cdots. \tag{23}$$

The numerical values of ΔG_V calculated by the use of the values of ν_0 in Table 1 are given in Table 8. By substituting the numerical values of Table 8 into eq. (25) and by means of the least square method, we have the following formula:

$$\Delta G_V=2342.18-122.992\ V+\frac{1}{2}\ +0.087664\left(V+\frac{1}{2}\right)^2. \tag{24}$$

Table 8.

The numerical values of ΔG_V

V	$\frac{1}{2}$	$1\frac{1}{2}$	$2\frac{1}{2}$	$3\frac{1}{2}$	$4\frac{1}{2}$	$5\frac{1}{2}$	$6\frac{1}{2}$	$7\frac{1}{2}$
ΔG_V	2220.2 cm^{-1}	2094.1 cm^{-1}	1982.4 cm^{-1}	1834.8 cm^{-1}	1745.2 cm^{-1}	1601.2 cm^{-1}	1484.6 cm^{-1}	1365.3 cm^{-1}

The vibrational constants of this state come out as follows:

$$\omega_e=2342.18\ cm^{-1}, \qquad 2\omega_e x_e=122.992\ cm^{-1}.$$

The $\Delta G_V : V$ curve for this state are shown in Fig. 3.

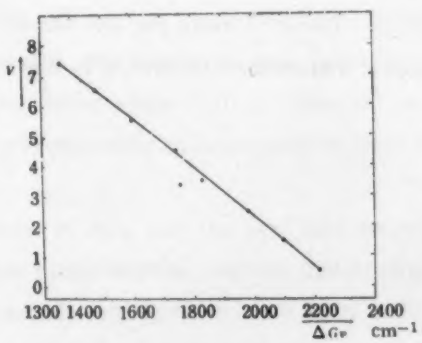

Fig. 3 $\Delta G_V : V$ for the D state.

4 Summary

The constants for the D state considered in this investigation are summari-

zed in Table 9.

Table 9.

The molecular constants of H_2 molecule in its $1s\sigma 3p\pi\,^1\Pi_{cd}$ state.

	e component level	d component level
B_e^x	30.519 cm^{-1}	31.942 cm^{-1}
α_e^x	1.5156 〃	1.6353 〃
γ_e^x	0.0057699 〃	0.03009 〃
D_e^x	−0.02371 〃	−0.02604 〃
β_e^x	0.00207 〃	−0.0009863 〃
H_e^x	3.2×10^{-5} 〃	3.2×10^{-5} 〃
I_e^x	0.91726×10^{-40} gcm^2	0.87640×10^{-40} gcm^2
r_e^x	1.0469×10^{-8} cm^{-1}	1.0233×10^{-8} cm
ω_e	2342.18 cm^{-1}	
$2\omega_e x_e$	122.992 cm^{-1}	

The perturbation and predissociation pointed out by Jeppesen and others were observed also in the present investigation at $v'=1$ and $v'=3$ respectively of the D state.

In the present case, however, the remarkable diffuse character at $v'=6$ of the D state as reported by Beutler and Jünger was not found.

In conclusion the writer wishes to express his heartfelt gratitude for Professor Yoshio Fujioka for his deep interest on the present work and for his kind permission to use the vacuum spectrograph of his own design. The writer wishes also to thank Dr. Yoshio Tanaka and Dr. Masao Seya for their valuable advice and many helpful suggestions presented to him throughout the course of the present work.

Band Spectra of Nitric Oxide in the Visible and Near Infra-red Regions.

Masaru OGAWA

Institute for Optical Research, Tokyo University of Education

(Received May 11, 1952)

Emission bands in the visible and the near infra-red regions were photographed, using electrical excitation of flowing NO gas. Vibrational analysis was made of two band systems among others. These band systems are shown to be due to the transition of $b \rightarrow B\ ^2\Pi$ (B being the upper state of the β-system) and $b' \rightarrow B\ ^2\Pi$ (b' being a new level) of the NO molecule. The results formerly obtained by Tanaka and Ogawa on the band spectra of NO in the visible region was corrected.

1 Introduction

Many reports[1~5] have been published on investigations of the spectra of nitric oxide (NO) in the visible and the near infra-red regions. The present author has recently reported[4] in collaboration with Tanaka that a system in the visible region was due to the transition between two upper states of the absorption spectrum of the NO molecule in the extreme ultraviolet region, namely between the upper states of P(I) and P(III)[6]. This report suggests that other sequences belonging to this system might be observed in the near infra-red region. More recently a study on the absorption spectrum of the NO molecule in the extreme ultraviolet region was made by Tanaka, Seya and Mori[7], who succeeded in finding several new progressions. According to this report, we might also expect several band systems to be observed in the visible and the near infra-red regions, corresponding to the transition between different excited states.

Since both the bands of NO_2 and the first and second positive groups of the nitrogen molecule are found in these regions, the experimental conditions of the previous investigations do not seem to have been quite suitable for the independent observation of the NO spectrum in these regions. In the present work,

1) L. Grillet and M. Duffieux: Compt. Rend., **201** (1935) 1338; 2) M. Duffieux and L. Grillet: Compt. Rend., **202** (1936) 937; 3) C. Jausseran, L. Grillet and M. Duffieux: Compt. Rend., **205** (1937) 39; 4) Y. Tanaka and M. Ogawa: Jour. of Sci. Res. Inst. **44** (1949) 1; 5) M. W. Feast: Canadian Jour. of Res., **28** (1950) 488; 6) Y. Tanaka: Sci. Pap. I. P. C. R., **39** (1942) 456; 7) Y. Tanaka, M. Seya and K. Mori: Science of Light, **1** (1951) 80.

the author took special precautions to observe the NO spectrum in the above mentioned regions in such manner as to be free of disturbance from the N_2 spectrum. The method of direct current excitation of flowing NO gas was utilized, which permitted, as was expected, the observation of numerous bands of the NO molecule.

2 Experimental Procedure and Appearance of the Spectrum

The discharge tubes used in this investigation were of the normal water cooled type with nickel electrodes in the form of hollow cylinders. We used two tubes of different sizes, one was 10 cm long with an inner diameter of 3 mm, and the other 12 cm by 1.5 cm diameter. For the discharge we had at our disposal two transformers, of respectively 20 kv, 1 kw and 3.3 kv, 5 kw capacity. The use of more powerful of the two transformers gave rise to the excitation of a spectrum of different appearance, and in the present work the smaller one was mainly used. To increase the intensity of the spectrum, the primary voltage was reduced to 50 v in order to provide a higher current density in the secondary circuit.

The spectrum between 9,000 Å and 3,500 Å was photographed by a glass spectrograph composed of three 60° glass prisms of 6 cm base. The focal length of the camera lens was 50 cm. The dispersion was about 46 Å/mm at 6,000 Å and about 77 Å/mm at 7,900 Å. The photographic plates used were Kodak 1-N for the near infra-red, and either Fuji panchromatic or Oriental hyper-panchromatic for the visible region.

As reported in our previous paper[1], we took special precautions for the gas, and used NO itself, for the preparation of which the same method as that described in that paper was used.

In the case of the first tube with smaller diameter, the greenish yellow glow with continuous spectrum, which is characteristic of air afterglow, extends as far in as the axis of the tube. This condition is not suitable for clear observation of the NO bands. We were able to avoid this by using the other tube and by adjusting the pressure and the rate of the flow of gas.

The electric current in the discharge tube and the rate of the flow of the gas were so adjusted that the first positive group of N_2 molecules formed by the

decomposition of the NO gas was absent in the visible region or at least very weak in the near infra-red region. The pressure of the gas to bring about such condition was about 10~18 mm Hg and the colors of the glow pink and greenish yellow. The pink glow was concentrated towards the axis of the tube, and the greenish yellow glow seen close to the wall of the discharge tube.

A sector in front of the slit of the spectrograph was sometimes used to avoid superposition of the continuum of the greenish yellow glow which followed after the main discharge. The sector was synchronized to open the slit simultaneously with the main discharge, which was repeated with a period of 6 cycles/sec, each flash lasting about 1/30 sec. This method was also useful in reducing the intensity of the N_2 bands, because with this arrangment the N_2 gas formed by the decomposition of NO was pumped out and replaced by a fresh charge of NO gas during the period of interruption before the occurrence of the next discharge.

The relation between the appearance of the spectrum and the gas pressure or the rate of the flowing gas, was the same as previously reported[4].

The time of exposure was about 40 minutes without the sector and about 2 hours with the sector for photographing the systems of $b \rightarrow B\,\Pi$ and $b' \rightarrow B'\Pi$, and 5~10 minutes for the strong but unanalysed bands arounds 8,600 Å and 7,800 Å.

The photographed spectra are shown in Plates 1 and 2, in which numerous bands may be seen. Some of them have four heads (the two stronger heads marked with vertical lines thus ‖ on the Plate) and are shaded towards the violet; these are considered to belong to one system. Naming these heads the first, second, third and fourth counting from the longer wavelength side, the first is weakest, the fourth the strongest, the third weak and the second stronger than the third. Other strong bands are found at 8,600 Å and 7,800 Å and a headless band at 6,000 Å. The 8,600 Å and 7,800 Å bands are groups of band heads, each of which bands degrades towards the shorter wavelength side.

When the pressure of the flowing gas was relatively low (say below 1 mm Hg) or the flow of the gas stopped, the above mentioned bands all disappeared, and were replaced by the first and the second positive groups of N_2 and the strong atomic oxygen lines (7,700 Å and 8,446 Å).

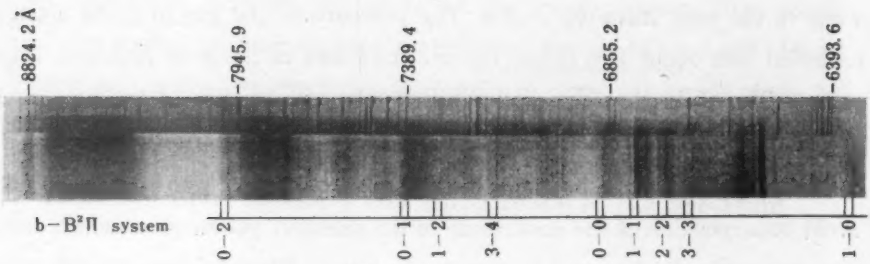

plate 1

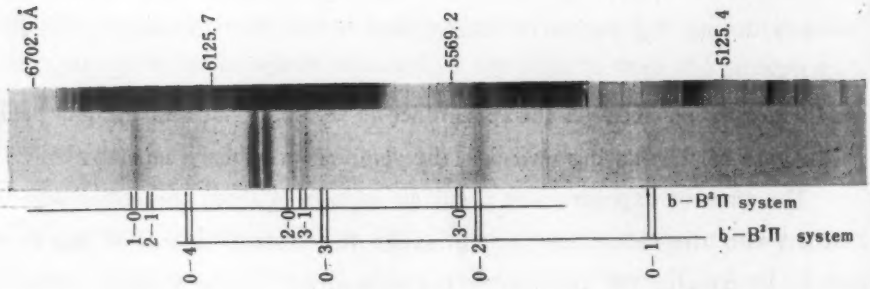

plate 2

3 Vibrational Analysis

The bands with four heads observed in the visible region, were considered by the author and Tanaka[4] to be the system corresponding to the transition between the upper states of the P(I) and P(III) progressions[6]. As mentioned already, some bands in the near infra-red region mutually possess a very similar appearance, though their observed wavelengths do not accord with the values calculated from the combination of the upper states of the P(I) and P(III) progressions. In spite of this disagreement however, the appearance of these bands is so similar that it could but be suspected that they belonged to one system. On this ground, vibrational analysis was again tried regardless of the

Table 1. $b \rightarrow B\,^2\Pi$ system

$v'-v''$	λ observed	ν observed	ν calculated	$v'-v''$	λ observed	ν observed	ν calculated
	8020.9	12464.0			6700.2	14920.8	
0–2	8010.5	12480.2	12482.6	3–3	6691.3	14940.7	14943.7
	7996.6	12501.9			6682.2	14961.0	
	7985.9	12518.6	12519.3		6673.3	14980.3	14980.4
	7420.2*	13473.6*			6377.8	15675.1	
0–1	7410.9	13489.9	13489.5	1–0	6369.6	15695.2	15696.2
	7401.1	13507.8			6362.3	15713.2	
	7389.9	13528.2	13526.2		6355.2	15730.8	15732.9
					6324.1	15808.2	
1–2	7313.9	13668.8	13667.4	2–1	6316.0	15828.4	15825.3
					6308.3	15847.8	
	7292.7	13708.6	13704.1		6302.5	15862.3	15862.0
	7170.1	13943.0					
3–4	7159.5	13963.8	13966.8	3–2			15935.6
	7149.7	13981.3					
	7140.1	14005.2	14003.5		6258.8	15973.1	15972.3
	6898.4	14492.1			5940.6	16828.7	
0–0	6889.3	14511.3	14511.4	2–0	5933.3	16849.4	16847.2
	6880.5	14529.8			5927.7	16865.3	
	6872.4	14547.0	14548.1		5921.4	16883.2	16883.9
	6811.8	14676.4	14674.3		5907.4	16923.2	
1–1	6806.4	14688.0		3–1	5900.0	16944.5	16942.5
	6796.7	14709.0	14711.0		5893.8	16962.3	
					5887.4	16980.7	16979.2
	6754.3	14801.3			5571.4	17943.8	
2–2	6746.4	14818.6	14818.4	3–0	5564.6	17965.8	17964.4
	6739.6	14834.5			5558.6	17985.2	
	6729.1	14855.4	14855.1		5551.3	18008.8	18001.1

Table 2. $b' \rightarrow B\,^2\Pi$ system

$v'-v''$	λ observed	ν observed	ν calculated
0–0			20113.0
			20144.1
			1023.3
			1021.7
0–1	5236.9	19089.9	19089.7
	5224.8	19134.2	19122.4
		1005.8	*1008.1*
		1015.7	*1006.6*
	5534.3	18064.1	
0–2	5528.2	18084.1	18081.6
	5522.6	18102.4	
	5517.7	18118.5	18115.8
		995.4	*992.9*
		993.2	*991.3*
	5856.2	17071.2	
0–3	5850.2	17088.7	17088.7
	5837.7	17125.3	17124.5
		980.0	*978.0*
		980.4	*976.1*
	6213.2	16090.3	
0–4	6206.1	16108.7	16111.1
	6196.7	16133.2	
	6192.3	16144.9	16148.4

conclusions previously attained by the authors.

The above analysis shows that the group does not belong to a single system but should be regarded as related to two distinct systems $b \rightarrow B^3\Pi$ and $b' \rightarrow B^3\Pi$. The state b is the one already known through the work of Tanaka, Seya and

Table 3.

Deslandres' table of $b \rightarrow B\,^3\Pi$ system (band heads)

v \ v''	0		1		2		3		4
0	14511.3 14547.0	*1021.4* *1013.8*	13489.9 13528.2	*1009.7* *1009.6*	12480.2 12518.6				
	1183.9 *1183.8*		*1186.5* *1180.8*		*1183.6* *(1190.0)*				
1	15695.2 15730.8	*1018.8* *1021.8*	14676.4 14709.0	*1007.6* *(1000.4)*	13668.8 (13708.6)				
	1154.2 *1152.4*		*1152.4* *1143.3*		*1149.8* *(1146.8)*				
2	16849.4 16883.2	*1021.0* *1020.9*	15828.4 15862.3	*1009.8* *1006.9*	14818.6 14855.4				
	1116.4 *(1125.6)*		*1116.1* *1118.4*		*1117.7*				
3	17965.8 (18008.8)	*1021.3* *(1025.1)*	16944.5 16980.7	*1007.6*	15973.1	*992.8*	14940.7 14980.3	*976.9* *975.1*	13963.8 14005.2

Mori[7], we shall here call b' the newly considered state similar to b. The wavelengths of related these two systems are listed in Tables 1 and 2. A Desladres' table of the first system ($b \rightarrow B^3\Pi$) is shown in Table 3. Both the strong heads (second and fourth) were used for the vibrational analysis. The difference of ΔG values obtained from the two heads coincided within experimental error and so the two were not treated separately. The wave numbers of these strong heads may be expressed by the following formula,

$$\nu_{v'v''} = \begin{matrix}14{,}422.9\\14{,}459.6\end{matrix} + 1{,}218.6\left(v' + \frac{1}{2}\right) - 16.9\left(v' + \frac{1}{2}\right)^2$$

$$- 1{,}036.9\left(v'' + \frac{1}{2}\right) + 7.5\left(v'' + \frac{1}{2}\right)^2.$$

The wave numbers calculated from this formula are noted in the last column of Table 1.

The obtained vibrational constants of the lower electronic state are found

to agree within experimental error with the values of $B^2\Pi$ state given by Jenkins, Barton and Mulliken[8]. The vibrational constants of the upper state appearing in the above formula differ from the values of the upper state of the B-progression of Tanaka, Seya and Mori (absorption spectrum of NO in the extreme ultraviolet region), but the observed $\Delta G_{v+1/2}$ values obtained here and from the B-progression are very close to the figure 5/2, as may be seen from Table 4. Moreover, the ν_{00} of $b \rightarrow X^2\Pi$ calculated from the ν_{00} of $b \rightarrow B\,\Pi$ and of the β-system ($B^2\Pi \rightarrow X^2\Pi$) are 60,034.2 and 59,906.0 cm^{-1} respectively, and these values agree well with the ν_{00} of the B-progression (Q heads). For these two reasons lead the author to believe that the present b state must be identical with the upper state of the B-progression, the observed disagreement between the two vibrational constants obtained from the present emission bands and the B-progression being due to the fact that in the calculation of the vibrational constants, $\Delta G_{v+1/2}$ in the former case covered the range 1/2 to 5/2, as contrasted to 1/2 to 9/2 in the latter case.

Table 4.

$\Delta G_{v+1/2}$ values of b state (in cm^{-1})

v / ΔG	0	1	2	3	4
$\Delta G_{v+1/2}$ from present work	1184.6	1152.2	1116.8		
$\Delta G_{v+1/2}$ from B-progression	1186.8	1152.8	1117.8	1059.8	1020.9

Only four bands were observed related to the second system. But their intervals agree with the ΔG values of the $B^2\Pi$ state. Hence, this system may be considered to correspond to the transition $b' \rightarrow B^2\Pi$. We calculated the ν_{00} of $b' \rightarrow B^2\Pi$ using the observed wave numbers of $b' \rightarrow B^2\Pi$ and the $G(v)$ values of $B^2\Pi$, and arrived at the values ν_{00}=20,144.1 and =20,113.0 cm^{-1}. Table 2 shows both the observed and the calculated values of the band heads (second and fourth heads) and the ΔG values. Although from the outward appearance of the spectrum, this b' level might seem to constitute a higher vibrational level of the b state, it does not coincide with any vibrational level obtained from the B-progression. Hence, this b' level does not belong to the b state but might be a new level.

8) F. A. Jenkins, H. A. Barton and R. S. Mulliken: Phys. Rev., **30** (1927) 150.

The $\nu_{00}(b'\rightarrow X^3\Pi)$ obtained from the $\nu_{00}(b'\rightarrow B^3\Pi)$ and the $\nu_{00}(B^3\Pi\rightarrow X^3\Pi)$ are 65,507.6 and 65,630.2 cm^{-1} respectively.

Acknowledgement

The author wishes to express his sincere thanks to Professor Yoshio Fujioka, director of the Institute, for his deep interests and valuable discussions upon the present work. He is also much indebted to Professor Yoshio Tanaka for his encouragement and valuable advise in the course of this work.

On the O_2 Atmospheric Bands Appearing in the Emission Spectrum.

Mitsuyoshi SHIMAZU

The Scientific Research Institute, Ltd.

(Received January 15, 1953)

The forbidden atmospheric oxygen bands were observed in the emission spectrum of pure oxygen, and of oxygen containing H_2O and N_2, both in the direct discharge and in the afterglow. Experimental conditions are described, and three spectrograms and a microphotometer curve are reproduced. Plausible mechanisms of the radiation processes are suggested.

1 Introduction

The atmospheric bands of oxygen molecule observable in the solar spectrum as the result of the absorption of the earth's atmosphere, are known to appear by the transition $b^1\Sigma_g^+ \leftarrow X^3\Sigma_g^-$. This transition is a forbidden one, and in laboratories the bands have been found in absorption under particular conditions. Recently, however, it was found that these bands could also be seen in emission. R. Herman and L. Herman[1], and G. Kvifte[2] observed the bands in emission in discharge through mixtures of rare gases and oxygen. R. C. Herman and his co-operators[3] observed the same bands in CO-O_2 explosion flames, and J. Kaplan[4] found them in the afterglow of particular cases of discharge. More recently, R. Herman and C. Weniger[5] observed them in experiments in high pressure discharge of pure oxygen, and L. M. Branscomb[6] in the direct discharge and afterglow of pure oxygen.

Again, these emission bands are observed in night sky light[7] and aurora[8], and it would seem very important to study the mechanism of radiation in order to clarify these phenomena in the upper atmosphere. The writer recently discovered that the atmospheric bands could be easily caused to be emitted in the so-called Wood tube discharge.

1) R. Herman and L. Herman: Comptes Rendus, **229** (1949) 931; 2) G. Kvifte: Nature, **168** (1951) 741; 3) R. C. Herman, H. S. Hopfield, G. A. Hornbeck and S. Silverman: Journ. Chem. Phys., **17** (1949) 220; 4) J. Kaplan: Phys. Rev., **71** (1947) 274; 5) R. Herman and C. Weniger: Comptes Rendus, **230** (1950) 940; 6) L. M. Branscomb: Phys. Rev., **86** (1952) 258; 7) A. B. Meinel: Astrophys. Journ., **112** (1950) 464; 8) G. Kvifte: loc. cit.

2 Experiment and Results

In the present experiment, two discharge tubes were used: one a Wood tube of 4 mm diameter having two electrodes separated by a distance of 150 cm, and the other a Π-type discharge tube of 25 mm diameter with electrodes 27 cm apart. A 3 KW, 40,000 volt transformer was used as source. The gases used were pure oxygen, electrolytic oxygen, tank oxygen, and various mixtures of oxygen and nitrogen. The pure oxygen was prepared by the heating of $KMnO_4$. The electrolytic oxygen and the tank oxygen were purposely not thoroughly purified in order to study the effect of impurities. The experiments were carried out at the pressure range of 0.5—30 mm Hg.

Since the atmospheric bands were never successfully obtained in the Π-type tube, nor with condensed discharge in the Wood tube, we will limit our description to the results obtained with the uncondensed Wood tube discharge.

The spectra were observed end on from 9000 A down to 1800 A in the central part (the portion of the positive column) of the Wood tube.

In the case of pure oxygen, the atomic lines of oxygen were present at about 0.5 mmHg, but no oxygen bands were then observed. When the pressure was raised, the intensity of atomic lines gradually increased, assuming maximum intensity at about 1.5 mmHg, when the atmospheric bands began to appear weakly. As the pressure was further increased, the atmospheric bands became stronger and took their maximum intensity at about 15—20 mmHg, while the atomic lines decreased gradually in intensity.

The tank oxygen, contained N_2 and H_2O as impurities, which caused hydrogen lines and the (0-0), and (1-0) bands of OH to appear strongly, together with bands of NO-γ in a wide range of pressure. The 1st and 2nd positive bands of N_2 appeared between 2 and 6 mmHg. Also in this case atmospheric bands were obtained from about 1.5 mmHg, and reached their maximum intensity at 15-20 mmHg, at which point they were as intense as in the case of pure O_2. Argon lines appeared from 0.5 to 30 mmHg, and were most intense at 0.5-1 mmHg above which they gradually decreased their intensity. In the experiments of R. Herman and others[1),2)], rare gases containing traces of oxygen were used, and the rare gases must in these cases have played an essential role. On the

other hand, in the present case, the tank oxygen contained only a very small percentage of argon, and the atmospheric bands appeared under almost the same conditions as in the case of pure oxygen. This would seem to indicate that in this case the argon did not play a role of any significance. The so-called air afterglow was intense in the case of tank oxygen and had its maximum intensity at about 5 mmHg.

In the case of the electrolytic oxygen, the lines of oxygen and hydrogen, and in particular the latter, were strong in the lower pressures. The atmospheric bands appeared in the pressure range of 1.5-30 mmHg, and as in the previous cases, assumed a maximum at 15-20 mmHg. It was remarkable that the intensity of the atmospheric bands came out so weakly when electrolytic oxygen was used. Also in this case no other oxygen bands were observed in the pressure range studied. As would be expected, OH bands in the ultraviolet region were very strong.

In Fig. 1 is shown the spectrogram of the direct discharge in tank oxygen taken with an exposure of 10 seconds on Eastman IN-plate* in a Zeiss "Licht-

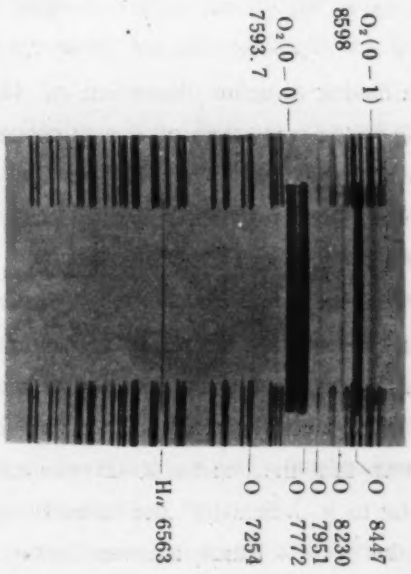

Fig. 1.

* The writer wishes to mention here that these Eastman infrared plates were the present of Profs. R. S. Mulliken and J. R. Platt of the University of Chicago and Dr. A. B. Meinel of the Yerkes Observatory for which he is most grateful.

stark" F/3.5 glass spectrograph. The (0-0) and (0-1) atmospheric bands appear clearly. In both bands P and R branches can be seen. The O lines at 7772 A and 8447 A were obtained very strongly.

In order to obtain more detail, some spectrograms were taken with an F/7

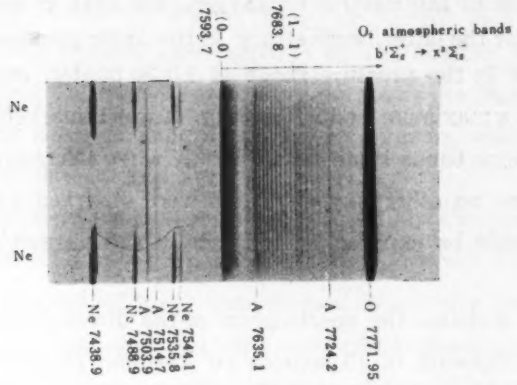

Fig. 2.

replica grating spectrograph having a higher dispersion of 45 A/mm. One of them is reproduced in Fgi. 2 which was taken of the discharge through tank oxygen at 15 mmHg with a 2 hour exposure. Apart from the (0-0) band, the (1-1) band can be clearly seen. The (2-2) band is not positive, its expected position being just masked by the strong 7772 A line.

The rotational structure of the P branch was well resolved, and so we ventured to study its intensity distribution with a microphotometer. The photograph was not taken wis an intensity scale, but the line of maximum intensity was used to determine the effective rotational temperature. From the microphotometer curve (Fig. 3), it is seen that the line for $J=12$ (upper state) has the maximum intensity. According to R. J. Schlapp[9] the intensity factor i for the P branch of the intercombination $^1\Sigma-^3\Sigma$ bands is given by $i=1/2(J+2)$. From this the intensity of the rotational lines is given by $I=Ci\exp[-BJ(J+1)/0.7T]$, and $B=1.40\text{cm}^{-1}$ for the atmospheric oxygen bands. In the present case, maximum

9) R. J. Schlapp : Phys. Rev., 39 (1932) 806.

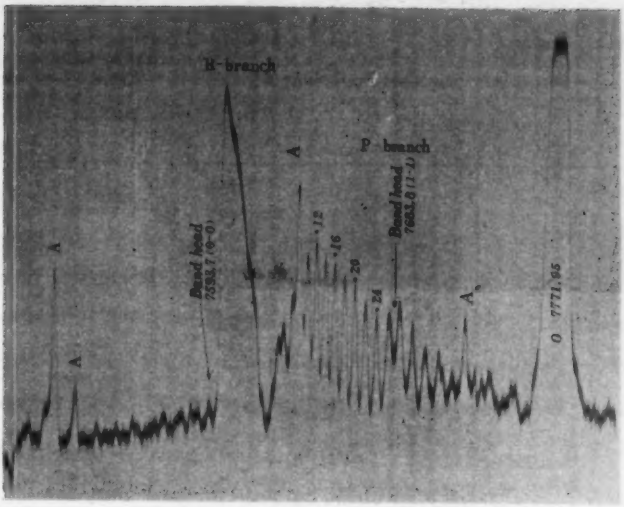

Fig. 3.

intensity is obtained at $J=12$, and accordingly the effective temperature is obtained as 700 °K. This value is very close to that given by Branscomb although the conditions of the present experiment could not be said to agree with that of Branscomb.

Next we studied the same bands in the afterglow spectrum of the uncondensed Wood tube discharge. This was studied by using a rotating sector which cut off the direct discharge. The atmospheric bands appeared in the afterglow with maximum intensity at about 15-20 mmHg. Under this condition the visible afterglow was hardly apparent. One of the spectrograms is reproduced in Fig. 4. In that figure the (0-0) and (0-1) bands can be seen clearly, unaccompanied by any O lines or other O_2 bands. Also seen is a continuous spectrum spread out between 9000 A and 7000 A, the origin of which is not clear, and might be attributed either to the air afterglow* (due to nitrogen impurity) or to a characteristic of oxygen or ozone.

Lastly, in order to study the effect of nitrogen upon the appearance of the atmospheric bands, we tried the experiment of using various mixtures of oxygen and nitrogen. When the percentage of nitrogen was increased, the intensity of

* Hitherto, the continuum of the air afterglow was believed to extend from 3700 to 6700 A. According to the writer's experiment (unpublished), however, it is certain that it extends up to about 10000 A.

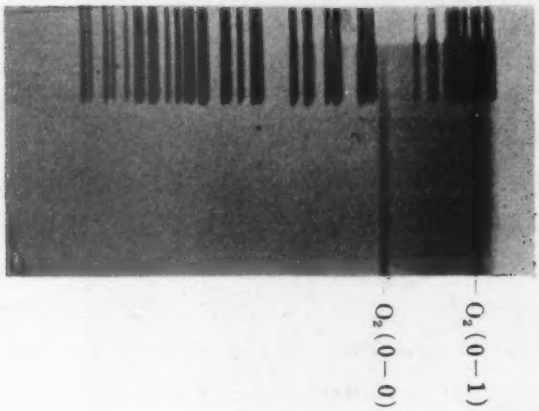

Fig. 4.

the atmospheric bands diminished their strength, though they could still be observed weakly in mixtures containing as much as 60 % nitrogen, at the total pressures of 10-15 mmHg.

3 Discussions

In the present experiment, it is found that the atmospheric bands appear in Wood tube discharge, where considerable atomic oxygen is expected to be present. Since the probability of exciting an oxygen molecule directly from its ground state ($X^3\Sigma_g^-$) to the upper state of the atmospheric bands ($b^1\Sigma_g^+$) must be said to be extremely small, it should be quite natural to assume that the oxygen molecule of the state $b^1\Sigma_g^+$ must have been produced by the mutual reaction of the discharge products including atomic oxygen. In other words, we must consider the occurrence of recombination or collision among the discharge products.

Several such processes are possible, and if we can calculate the probability of each processes we shall be able to predict the most probable one by comparing these values. To do this, further studies of the energy levels of the oxygen atom and molecule and more detailed calculations on the cross-sections of the collision processes seem to be necessary. Unfortunately however, both experimental and theoretical data are so scarce that we must wait until further investigations have been made. Therefore the following paragraphs the discussions will be pursued

only from the standpoint of the energy levels.

(1) Two body radiative recombinations.

Firstly, we consider that the molecular state which combines with the $b^1\Sigma_g^+$ state by dipole transition and which results from recombination of two normal oxygen atoms (^3P) must be a $^1\Pi_u$ state, which has not yet been found. Since the dissociation limit of $O(^3P)+O(^3P)$ is about 5 e. V., if we assume that this state has a potential curve which is repulsive at the position vertically above the minimum point of the potential curve of the $b^1\Sigma_g^+$ state, a continuous spectrum must be expected near 3700 A. However, this continuum was not observed in the present experiment, so this process seems to be improbable.

Since from the recombination of $O(^3P)+O^*(^1D)$, and $O(^3P)+O^*(^1S)$, we cannot expect any state that combines with the $b^1\Sigma_g^+$ state by dipole transition, these processes may be omitted from further consideration.

From two excited oxygen atoms $O^*(^1D)$ we have two $^1\Pi_u$ states which combine with $b^1\Sigma_g^+$ state by dipole transition. If these states are repulsive at the position vertically above the minimum point of the potential curve of the $b^1\Sigma_g^+$ state, we should have a recombination continuum in the vacuum ultraviolet region. If we can confirm this continuum the radiative recombination of two $O^*(^1D)$ atoms will be a probable process for the production of the $b^1\Sigma_g^+$ state. Unfortunately, we were not enabled to investigate this range of wavelength in our present experiment. Neither will these states be easily observed by absorption, because the ground state of the oxygen molecule is $^3\Sigma_g^-$.

In the same manner, we may consider $^1\Sigma_u^+$ and $^1\Pi_u$ molecular states resulting from two excited oxygen atoms $O^*(^1D)$ and $O^*(^1S)$ and which combine with the $b^1\Sigma_g^+$ state by dipole transition. Therefore the radiative recombination of $O^*(^1D)$ and $O^*(^1S)$ will also be considered to be a probable process for the production of the $O_2^*(b^1\Sigma_g^+)$ state. However in this case too, the recombination continuum must appear in the extreme ultraviolet region beyond our power to confirm, and for the same reason as before, these excited states will not be observed by absorption.

(2) Two body inelastic collision.

It is known that O_2 is produced in the positive column of the glow discharge

of oxygen,[10] so it may naturally be considered that O_3 will be present in our discharge tube, which would emit the atmospheric bands. This leads us to consider the possibility of the $b^1\Sigma_g^+$ state being produced by the reaction

$$O_3 + O(^3P) \rightarrow 2O_2^*(b^1\Sigma_g^+) + 0.7 \text{ e. V.}$$

This process seems to be a plausible explanation for the experimental facts that the atmospheric bands appear only in discharges in which high concentration of atomic oxygen is believed to exist, and that these bands are not observed with the violent discharges in which O_3 would decompose. Also, in view of the fact that water vapor very much affects the production of O_3, the above mechanism will explain the experimental result that atmospheric bands appear very weakly with the use of electrolytic oxygen not thoroughly dried. It also explains the occurrence of atmospheric bands in the afterglow.

(3) *Three body recombinations without radiation.*

We will now consider the three body collision involving O_3

$$O_3 + O(^3P) + O(^3P) \rightarrow O_2(X^3\Sigma_g^-) + O_2^*(b^1\Sigma_g^+) + O^*(^1D) + 0.42 \text{ e.V.}$$

At a first glance, this process would seem to explain well the observed phenomena, but a further scrutiny would reveal its improbability because there is no substance to deactivate the metastable $O^*(^1D)$ atom, the forbidden red auroral line 6300 A should appear according to the process $O^*(^1D) \rightarrow O(^3P) + h\nu$, and this is not the case in the present experiment.

The other three body collision

$$O(^3P) + O(^3P) + X \rightarrow O_2^*(b^1\Sigma_g^+) + X^*(3.5 \text{ e.V.})$$

may also be considered as a plausible process. In the case of the discharge in pure oxygen, however, it is difficult to presume an X which would fulfil the above relation. But in the case where nitrogen was present, the metastable nitrogen atom ^2P might be considered for this X, since the excitation energy of the ^2P state is 3.57 e. V.

In the present experiment, it is uncertain whether or not the above process is responsible for the occurrence of the atmospheric bands when the nitrogen is contained as impurity.

10) A. K. Brewer and J. W. Westhaver: Journ. Phys. Chem., 34, 1 (1930) 1280;

Kaplan[9] has observed atmospheric bands for the first time in the afterglow emission of special discharge. In this case the above process may play an important role.

(4) Collisions involving electron and negative ions.

It is known that, in the glow discharge in electro-negative gases and vapors, considerable negative ions are formed,[11] which affect considerably the character of the electric discharge. It is very interesting to note that if we take negative ions into account, the following processes may be considered plausible for the production of the $O_2^*(b^1\Sigma_g^+)$ state. Assuming the electron affinity of oxygen atom to be 2.2 e. V., the three body collision including electron,

$$O + e + O_2 \rightarrow O_2^*(b^1\Sigma_g^+) + O^- + 0.6 \text{ e.V.}$$

will explain the occurrence of atmospheric bands in the direct discharge and in the afterglow. Another process may be considered:

$$O_2^- + O \rightarrow O_2^*(b^1\Sigma_g^+) + O^- + 0.3 \sim 0.5 \text{ e.V.}$$

where the energy to detach an electron from O_2 molecule is assumed to be 0.1 -0.3 e. V.[12],[13] The latter reaction may also explain the phenomena observed in laboratories. Since the electron energy will not be so large at 15-20 mmHg, this attachment process might be considered possible, and though, as stated above, the energy to detach an electron from O_2 is relatively small, many negative ions, may still exist under discharge conditions of 15-20 mmHg and 700°K (see above), as is confirmed by a rough estimation. As described above, H_2O as impurity seems to weaken the atmospheric bands, the reason for which probably is that the electro-negative character of H_2O affects the above two processes.

Although the mechanisms suggested above will not necessarily have direct connection with phenomena in the upper atmosphere, they seem to explain considerably well the phenomena observed in the present experiment.

In conclusion the author expresses his sincere appreciation for the kind guidance and encouragement extended to him throughout the course of this work by Professor Yoshio Tanaka of the Tokyo University of Education. The author also feels very grateful to Professor Yoshio Fujioka for his many valuable suggestions.

11) H. S. W. Massey: *Negative Ions* (1938), Cambridge Physical Tracts; 12) L. B. Loeb: Phys. Rev., **48** (1935) 684; 13) N. E. Bradbury: Phys. Rev., **44** (1933) 883.

On the PbS Photoconductive Cell

Noboru SASSA

Department of Physics, Aichi Liberal Arts University

and

Masatoshi NAKAMURA

Institute for Optical Research, Tokyo University of Education

(Received Dec. 12, 1952)

PbS photoconductive cells were prepared by the evaporation method and their dark resistance, sensitivity, time constant, spectral response and other characteristics were measured. The sensitivity was found to be 1.9×10^{-10} W and the time constant 3×10^{-4} sec. (at room temperature).

The above performance is considerably better than that of detectors hitherto used and should permit the use of this cell as near infrared detector.

Introduction

The preparation of an infrared detector with high sensitivity and stability is of great importance in all branches of infrared study and for this purpose use has mainly been made in the past of the thermopile and the bolometer, but recent developments in electronic technology have replaced the galvanometer by the amplifier-recorder system. In the present instance, a detector was called for which would not only be selective and stable but also have a small time constant, and from this stand-point the thermopile or the bolometer could not be considered satisfactory.

The PbS photoconductive cell, discovered by Bose back in 1901, has recently been developed as a detector, to which attention was attracted because of its small time constant and high sensitivity, although its response is limited to the near infrared. Its characteristics have been investigated by Sutherland[1], Schwarz[2], Moss[3], Gibson[4] and many others, while Jones[5], Fellgett[6] and Moss[7] have calculated the limiting sensitivity of radiation detectors, and it has been concluded that the photoconductive cell is superior to the thermopile or the bolometer, with

1) G. B. B. M. Sutherland, D. E. Blackwell and P. B. Fellget; Nature **158** (1946) 873; 2) E. Schwarz; Nature **162** (1948) 615; 3) T. S. Moss: Nature **159** (1947) 476; 4) A. F. Gibson: Proc. Phys. Soc., B64 (1951) 603; 5) C. Jones; Juor. Opt. Soc. Amm. **37** (1947) 879; 6) P. Fellgett; Juor. Opt. Soc. Amm. **39** (1949) 970; 7) T. S. Moss; Juor. Opt. Soc. Amm. **40** (1950) 603.

respect to sensitivity and time constant, although the latter two possess the advantage of being homogenious in sensitivity against the wavelength.

The present paper deals with the time constant, the sensitivity and the spectral response of the PbS cell, together with the temperature dependence of its electrical conductivity.

1 Preparation of PbS Cell

Two methods are known for the preparation of the PbS photoconductive cell, namely the methods of evaporation and of chemical deposition. We prepared the cell by the former method*.

Two pieces of tungsten were sealed in one end of a hard glass tube and aquadag was backed in the inside wall of the tube to form the electrode. The outline of the cell is shown in Fig. 1.

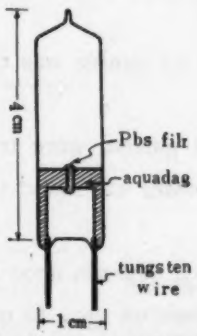

Fig . 1 Outline drawing of the Cell. Aquadag is coated inside the glass tube as the electrode and PbS film is deposited between the both electrode.

The evaporating materials used in our experiment were PbS and PbS_2O_3 powders and galena. About 2～3 mg of one material was inserted in the cell. The cell was pumped with a vacuum leak, the pressure being kept at 0.1～1 mmHg and the material was evaporated under this pressure by a gas flame. The material was moved by successive evaporation until it filled the space between the electrodes. After this process the photoconductivity of this cell was roughly tested, the material being reevaporated when the cell was not found to be sufficiently sensitive. The cell thus prepared was placed in an oven, and measurements made of the variation of its conductivity with rising temperature. The conductivity was found to increase with the temperature up to 380°C, after which it decreased again. The cell was taken out at this critical temperature and left to cool down to room temperature, upon which the vacuum leak was closed and the cell was pumped and sealed off at the pressure of 10^{-4} mmHg.

* The writers are very grateful to Professer Sutherland who kindly presented one of his own cells to Professer Fujioka as a sample.

2 Condition to Increase Sensitivity

In order to obtain as high sensitivity as possible, we took special precautions in (1) the cleaning of the glass wall, (2) control of air flow during the evaporation and heat treatment, (3) control of the air pressure, (4) selection of the evaporating materials, (5) quantity of the materal, (6) rate of evaporation and (7) heat treatment after the evaporation.

(1) It was found that the cleaning of the glass wall had an important effect on the sensitivity. When the wall was not sufficiently cleaned, it was difficult to obtain a high sensitivity.

(2) The passing of air or oxygen during evaporation is intended to remove harmful reaction products such as SO_2[8] and thus to increase the sensitivity. However, we were not successful in precisely determining the effect of air flow, though we experimented with different rates.

(3) As regards air pressure, it was found the 0.6 mmHg was the most suitable for best results.

(4) Three kinds of materials, PbS, PbS_2O_3 and galena, were tried, the former two having been chemically precipitated. PbS powder was found to be the best.

(5) The quantity of the material to be evaporated depends upon the size of the tube, the pressure of the air, the rate of evaporation etc.. In our case, where a tube of 3~4 cm in length by 1 cm diameter was used 2~3 mg of the material was found to be the optimum quantity for obtaining high sensitivity.

(6) A general rule for the proper rate of evaporation could not be determined, but when fixed proper values for the quantity of the material, the pressure of the air and the size of the tube were given, there was seen to be an optimum rate. When the evaporation took place at this velocity, it appeared that the crystal grains were precipitated in the most appropriate size and the most suitable oxide film[9] was formed on the surface of the grain. However, we were not able to determine quantitatively such a condition.

(7) The heat treatment has the function of stabilizing and senstizing the

8) V. K. Zworykin and E. G. Ramberg: "*Photoelectricity*" New York, John Willy and Sons Inc. 1949. London Champan and Hall Limited; 9) See reftrance 4);

product. The evaporation process produces many unstable crystallin grains, and the heat treatment is necessary for stabilizing the PbS film as a detector. On the other hand, heat treatment in low pressure air (0.1～1 mmHg) has some effects on the sensitivity owing to adsorption and desorption of oxygen on the grain surface and to the change in impurity (the replacement of F-center by O^{--} ion[10]). In our experiment the sensitivity was generally found to increas by the heat treatment, and exceptional cases of deterioration were due to excessive heating. Fig. 2 shows the temperature dependence of the conductivity. In this

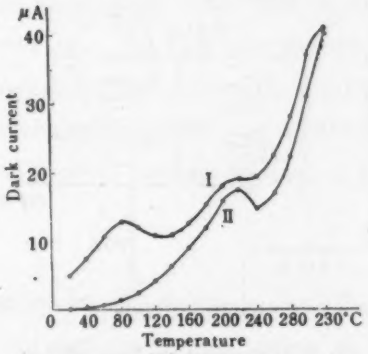

Fig . 2 Temperature Dependence of the Conductivity of PbS Film.
Longitudinal axis shows the current through the PbS film at applied voltage 1.5 volts.
I: Curve obtained immediatly after preparation at 0.1 mm Hg pressure of air.
II: Curve obtained by heating in air of 0.075 mm Hg pressure about 12 hours after the curve I was obtained.

figure, the ordinate represents the current (proportional to σ) at an applied voltage of 1.5 V and the abscissa is the temperature in degrees centigrade. As can be seen from this figure, the relation between the conductivity and the temerature is not so monotonous as to be attributed to a simple electronic process, but would appear also to involve the so-called atomic process, which prevented us from being able to analyse the results quantitatively at the present stage.

10) W. Ehrenberg and J. Hirsch: Proc. Phys. Soc. **B64** (1951) 700.

3 Measurement of Characteristics

In order to obtain the characteristics of the cell prepared as avobe, we measured its dark resistance, linearity for illumination, sensitivity, time constant, spectral response etc..

The amplifier system which was used throughout the experiments is partly diagrammed in Fig. 3. This layout is a modification of Ritther's circuit[11] and was employed as a pre-amplifier. It was connected with a two stage R-C coupling

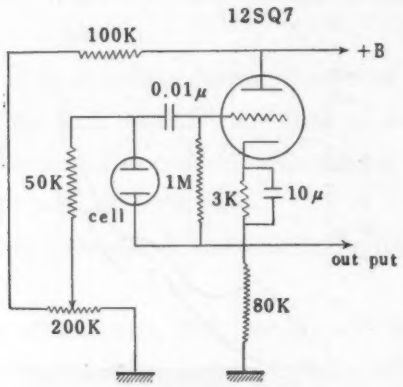

Fig. 3 Diagram of the Pre-Amplifier Circuit.
This is a modefication of E. Ritter's circuit.

amplifier. In measuring the output, a vacuum tube voltmeter with diode rectifier was used in order to measure peak height The illumination could be interrupted at any frequency between 50~2000 cycles by a mechanical chopper.

A) Resistance (Dark)

The measurement of the dark resistance was carried out by using a Wheatstone bridge in a dark room. The resistance ranged from 0.1 MΩ to 20 MΩ, 1 MΩ being found to be the most frequent.

B) Linearity for Illumination

A good linearity between the response of the cell and the intensity of radiation is demanded to permit application of the PbS cell to photometry, and the following method was employed for checking this characteristic. A tungsten

11) E. Rittner: Rev. Sci. Inst. 18 (1947) 36.

lamp was used as light source, and the relative intensity of illumination was determined by changing the distance between the light source and the cell, sliding the source on a 3 meters optical bench. The response of the cell corresponding to the distance was measured.

The cell was connected to a dry battery of 9.3 V and a micro ammeter in series, and a tungsten lamp of 100 V- 200 W was used as light source. Fig. 4 shows one of the results, illustrating that linearity is confined to intensities under 30 milli lumens/cm^2.

Next we made the same experiment using an amplifier. For light source, a 100 V-40W tungsten lamp was used at the applied voltage of 20 volts in order to reduce the intensity of illumination. The result, as is seen in Fig. 5, indicates that its reponse was linear up to the light intensity of 10 μW/cm^2. For a higher intensity the linearity seemed to break down due to deformation in the last stage of the amplifier. To overcome this defect, we need only to reduce the gain of amplifier, but we did not proceed further, because it was beyond the range of the experiment.

C) Sensitivity

To measure the sensitivity, the fluctuation and the response of the cell was measured when it was exposed to the illumination of a standard electric lamp (voltage 90.3 V, current 0.351 A, colour temperature 2355°K, radiation density at 1 meter 8.3 μW/cm^2). The sensitivity was determined by the energy necessary to record the same deflection as the fluctuation. It was found that our best cell had the sensitivity of 1.9×10^{-10} watts at room temperature.

D) Time Constant

Theoretical considerations and experimental measurements on the time constant of the PbS cell have been carried out by Gibson[12]. According to him the time constant varies with respect to the temperature as well as to the intensity and pulse length of the illumination. In order to measure the time constant, we changed the rate of the revolution of the chopper. When the speed is sufficiently slow, the output response of the cell is constant, but it decreases gradually as the frequency rises above a certain value. The time constant is given by the illumination time at the stage where the output response decreases

12) See referance. 4).

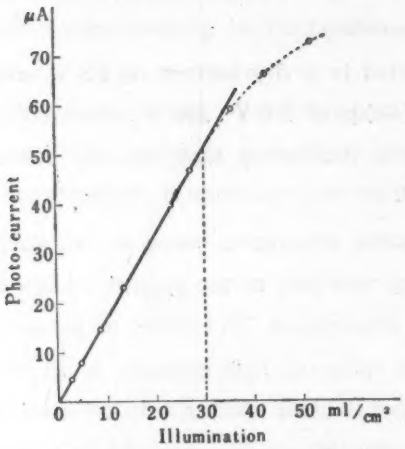

Fig. 4 Linearity of the Cell for Illumination. Photo-current of the cell at applied voltage 9.3V was measured by changing the intensity of illumination.

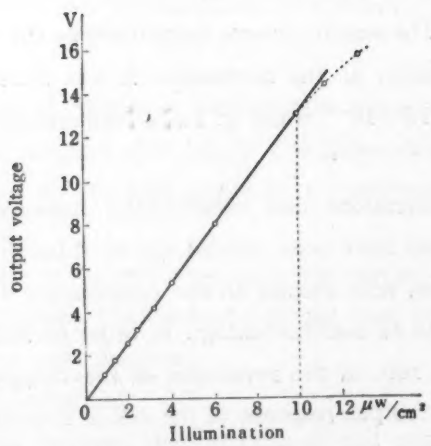

Fig. 5, Linearity of the Cell Connected to the Amplifier for Illuminaton. Longitudinal axis shows the output voltage of the amplifier.

to $(1-e^{-1})/(1+e^{-1})$. The result for one of the cell is 2.8×10^{-4} second (at 15.5°C), as shown in Fig. 6. In this figure, are given the results of two experiments on one and the same cell, with slight change of the intensity of the illumination, and it is seen that the two results are almost identical. Several experiments of the same kind for other cells have produced results approximately the same, that is, around 3×10^{-4} sec.

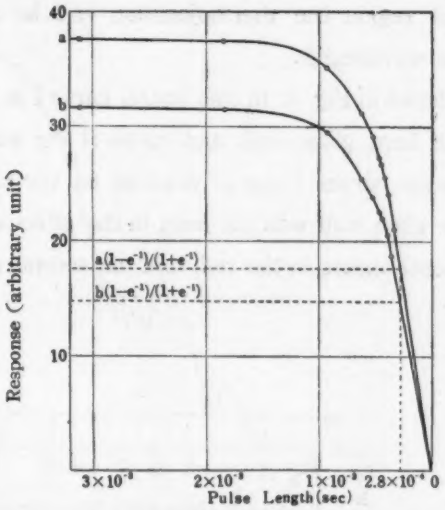

Fig. 6. Reponse of the Cell for the Square Wave Illumination. The responses of the cell were measured, changing the pulse length of the illumination. Two curves were obtained for the same cell by changing slightly the intensity of illumination. a and b are the values of responses for suffciently long pulse illumination and horizontal doted lines are $(1-e^{-})/(1+e^{-1})$ times a and b respectively. The time constant was determined from the value of the pulse length which corresponded to the cross point of the horizontal doted line with the observed response curve.

E) Spectral Response and Application

To investigate the the spectral response and the possibilities of application to the spectrometer, we used an infrared spectrometer consisting of a rock salt prism, a spherical collimating mirror with a focal length of 50cm and two plane mirrors arranged in the Wadsworth-Littrow system. The light beam emerging from the exit slit was interrupted at 380 cycles per second by a mechanical chopper, and the voltage caused in the PbS cell was amplified by the pre ampli-

fier described above and an a. c. amplifier tuned to the same cycle as the chopper. A galvanometer with low sensitivity was used instead of a micro ammeter attached to the vacuum tube voltmeter and the deflection of the galvanometer was recorded on a rotating drum.

To obtain the spectral reponse of the PbS cell, we compared the sensitivity of the PbS cell with that of a thermojunction. The ratio of the output of the PbS cell to that of the thermojunction gives the spectral response of the cell, since in the near infrared region the thermojunction can be considered uniformly sensitive against the wavelength.

The result is shown in Fig. 7. In this figure, curve I is the spectral response of the PbS cell with hard glass wall, and curve II the same with quartz wall. The difference between curves I and II depends on the character of each cell, and the effect of the glass wall was not seen in the effective region of PbS cell. The maximum response exists in the red, and the second peak appears roughly

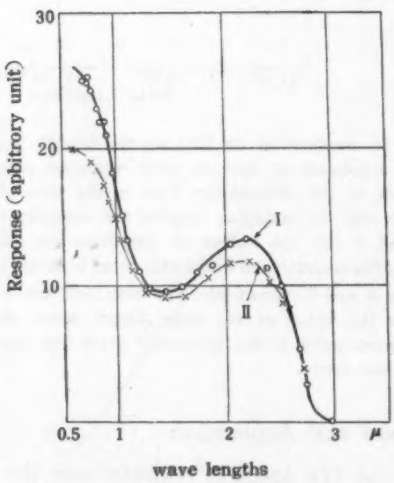

Fig. 7 Spectral Response of the Cell.
I. With the wall made of the hard glass.
II. With the wall made of the quartz.

at 2.3 μ. It was noticed that in some cases the maximum occurred at the longer wave length.

As the PbS cell is much more sensitive than the thermojunction in the near infrared region, we tried its use as the detector of an infrared spectrometer, in which we used a glass prism instead of a rock salt prism. It permits the

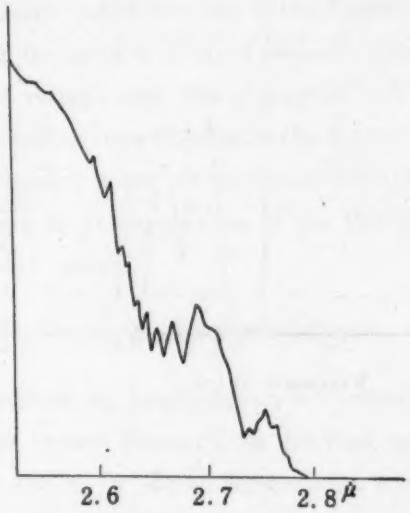

(A) Detector : PbS Photoconductive Cell
Slit width : 0.04 mm

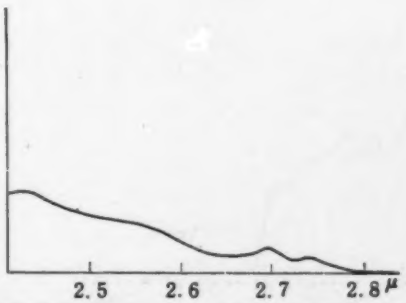

(B) Detector : Thermo-junction ($3.3\mu V/\mu w$)
Galvanometer ($5\times10^{-8}v$)
Slit width : 0.3 mm

Fig. 8. Absorption Spectra of H_2O (2.72μ) and CO_2 (2.69μ) Contained in Atmospheric Air.

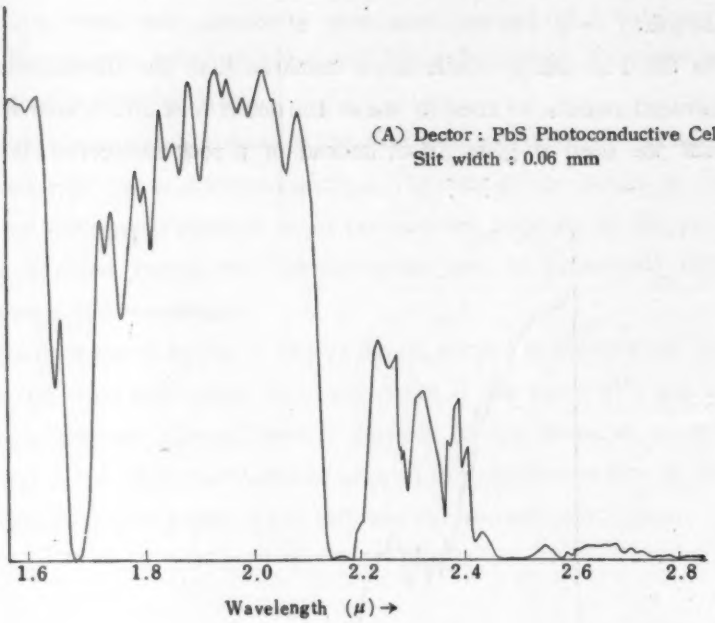

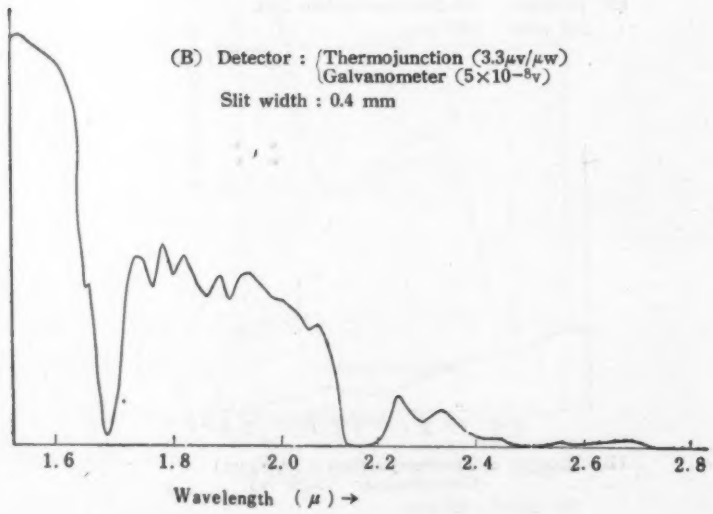

Fig. 9 Absorption Spectra of Liquid Benzene.

width of the slit to be made considerably narrower than in the case of the thermojunction, which results in high resolution of the spectrometer.

Fig. 8A is a spectrum obtained with the use of the PbS cell as a detector, showing the absorption bands of H_2O (2.72 μ band) and CO_2 (2.69 μ band) contained in atmospheric air. Fig. 8B is the same spectrum obtained with a thermojunction (sensitivity 3.3 μV/μW) connected to a galvanometer (sensitivity 5×10^{-8} V/mm). The slit widths were 0.04 mm in the former and 0.3 mm in the latter. Figs. 9A and B are the spectra of liquid benzene, obtained with the PbS cell and the thermojunction respectively. The absorption cell is 3 mm in thickness for each case. The slit widths were 0.06 mm in the former and 0.4 mm in the latter. From above experiments, it may be concluded that the slit width can be reduced roughly to one tenth by the application of the PbS cell in place of the thermojunction-galvanometer system.

4 Acknowledgment

We wish to express our hearty thanks to Professor Yoshio Fujioka, Director of the Institute for Optical Research, for his kind encouragement and guidance in this work, and also, to Dr. Masao Seya and Dr. Ryumyo Ito for their valuable help and kind advice.

On the Interference Filter.

The Characteristics of the Alternating Layer Type Interference Filter

Minoru IWATA

Osaka Industrial Research Institute

(Received Dec. 10, 1952)

The author[1] has previously calculated the reflection curves of the alternating layer type interference filters having up to ten layers. The present report is a general treatment of the above type of filter with a further large number of layers, performed with application of the electrical network theory, and in this instance, that of an iterative four terminal network, which was found to be perfectly suited for the purpose.

The conclusions obtained were as follows:

i) The reflection spectrum should prove to show strong maxima with definite widths.

ii) The widths of the maxima are determined by the refractive indices of each alternating layer.

Introduction

In the previous paper, reflection curves of alternating layer type interference filters having up to ten layers were obtained by calculation. Now, when the number of layers is further increased, the calculation of the reflection curves becomes extremely complicated.

Schelkunoff[2] pointed out the possibility of applying of the electrical network theory and the methods thereof to problems of the electromagnetic field. Problems in the reflection and transmission of electromagnetic waves were solved along this line by Stratton[3] and Muchmore[4] for the cases respectively of single and double layered thin films.

It was recoginzed by the author that the theory of the iterative four terminal network was perfectly suited to solve the problem of reflection by alternating layers of any number.

Details of the calculation are discussed in the following pages, together with a discussion on agreement with some experimental results. In (1) is described the application of the electrical network theory to the problem of thin films. In (2) the reflection formula for alternating layers of any given number

1) M. Iwata: Tech. Report of the Osaka Industrial Research Institute, Special Number, (March 1950); 2) S. A. Schelkunoff: Bell System Tech. J. **17**, 17 (1938); 3) J. A. Stratton: "Electromagnetic Theory" (McGraw-Hill Book Co., New York, 1941), pp. 511-516; 4) R. B. Muchmore: J. O. S. A. **38**, 954 (1948).

is derived by applying the theory of iterative four terminal networks. (3) and (4) are devoted to the discussion of the characteristics of the reflection formula, and in (5) some experiments to substantiate the results are described. In (6) may be found some suggestions for the application of the results obtained.

1 Application of the Electrical Network Theory to the Problem of Thin Films

An excellent method of computation of the reflectivity and transmissivity of multilayerd thin films was given by Weinstein[5]. The following is an abstract of the portions of his paper having direct bearing on our subject.

The discussion is initiated with a set of equations expressing the boundary conditions which must hold between the various electromagnetic waves at the film interfaces. We shall consider the case where the electric intensity vector of the incident light is perpendicular to the plane of incidence. (The case where the electric intensity vector of the incident light is parallel to the plane of incidence is easily solved by analogy). It will be assumed that there are $p+1$ media and quantities belonging to these shall be given subscripts 0 to p.

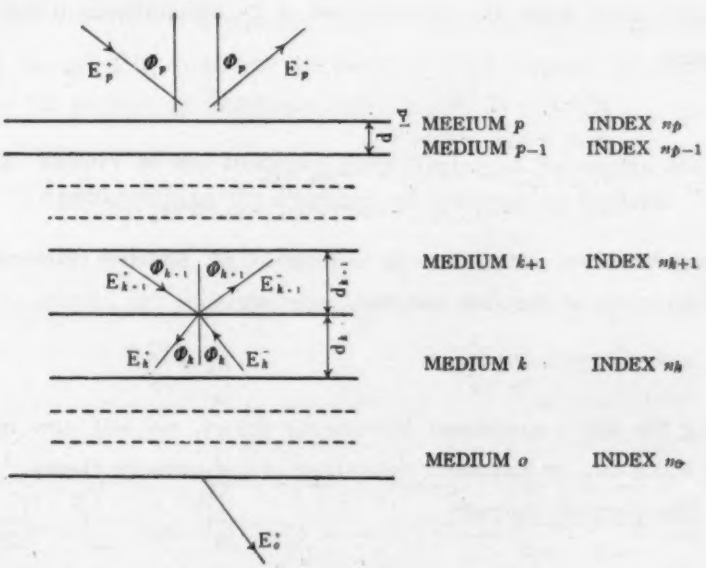

Fig. 1.

5) W. Weinstein: J. O. S. A. 37, 576 (1947).

Let the symbols be:

n_k refractive index of medium k ($k=0, 1, 2,\cdots\cdots,p$)

d_k thickness of medium k ($k=1, 2, 3,\cdots\cdots,p-1$)

E_k^+ amplitude of electric intensity vector in the beam travelling in the positive direction in medium k ($k=0, 1, 2,\cdots\cdots,p$)

E_k^- amplitude of electric intensity vector in the beam travelling in the negative direction in medium k ($k=0, 1, 2,\cdots\cdots,p$)

ϕ_k angle of incidence in the positive direction in medium k ($k=0,1,2,\cdots\cdots,p$)

λ wave length of the incident light in vacuum.

The relevant boundary conditions are that the tangential components of the electric and magnetic intensity vectors should be continuous at each interface.

We put,

$$\begin{cases} v_k=(2\pi/\lambda)n_k\cos\phi_k, \\ y_k^+=E_k^+\exp\{iv_k(d_{p-1}+d_{p-2}+\cdots\cdots+d_k)\}, \\ y_k^-=E_k^-\exp\{-iv_k(d_{p-1}+d_{p-2}+\cdots\cdots+d_k)\}, \\ w_k=n_k\cos\phi_k. \end{cases}$$

$$(k=0, 1, 2,\cdots\cdots,p)$$

If the two boundary conditions for each interface are set forth, and the above substitutions made, the following set of $2p$ simultaneous linear equations are obtained.

$$\begin{cases} y_1^+ + y_1^- - y_0^+ = 0 \\ w_1y_1^+ - w_1y_1^- - w_0y_0^+ = 0, \\ y_{k+1}^+ + y_{k+1}^- - e^{-iv_kd_k}y_k^+ - e^{iv_kd_k}y_k^- = 0, \\ w_{k+1}y_{k+1}^+ - w_{k+1}y_{k+1}^- - w_ke^{-iv_kd_k}y_k^+ + w_ke^{iv_kd_k}y_k^- = 0. \end{cases} \tag{1}$$

These must be solved for y_p^+ and y_p^- in terms of y_0^+, and the transmissivity T_p and reflectivity R_p of the film are then given by

$$T_p=\frac{n_0}{n_p}\left|\frac{y_0^+}{y_p^+}\right|^2, \qquad R_p=\left|\frac{y_p^-}{y_p^+}\right|^2. \tag{2}$$

Using the above mentioned Weinstein's theory, we will now deduce the variables which can be compared with those of the network theory.

For this purpose we put:

$$\begin{cases} y_k^+ + y_k^- = f_k, \\ w_ky_k^+ - w_ky_k^- = g_k. \end{cases} \tag{3}$$

Eqs. (1) may be written as follows·

$$\begin{cases} f_1-f_0=0, \\ g_1-g_0=0, \\ f_{k+1}-f_k\cos(v_kd_k)+i\dfrac{g_k}{u_k}\sin(v_kd_k)=0, \\ g_{k+1}+iw_kf_k\sin(v_kd_k)-g_k\cos(v_kd_k)=0. \end{cases} \tag{4}$$

Then

$$\begin{cases} f_k=f_{k+1}\cos(v_kd_k)+\dfrac{g_{k+1}}{u_k}i\sin(v_kd_k), \\ g_k=w_kf_{k+1}i\sin(v_kd_k)+g_{k+1}\cos(v_kd_k) \end{cases} \tag{5}$$

Eqs. (5) may be expressed in the form of a matrix.

$$\begin{pmatrix} f_k \\ g_k \end{pmatrix}=\begin{pmatrix} \cos(v_kd_k) & \dfrac{i}{w_k}\sin(v_kd_k) \\ iw_k\sin(v_kd_k) & \cos(v_kd_k) \end{pmatrix}\begin{pmatrix} f_{k+1} \\ g_{k+1} \end{pmatrix}. \tag{6}$$

Eq. (6) is identical with the fundamental equation of a four terminal network

$$\begin{pmatrix} E_k \\ I_k \end{pmatrix}=\begin{pmatrix} A & B \\ C & D \end{pmatrix}\begin{pmatrix} E_{k+1} \\ I_{k+1} \end{pmatrix}. \tag{7}$$

where E_k and I_k are the voltage and the cuurent respectively at the terminal (k, k). A, B, C and D are the so-called four terminal network constants and have the relation $AD-BC=1$. Comparing Eq. (7) with Eq. (6) we may see that by replacing E_k and I_k by f_k and g_k the theory of four terminal networks may be applied to the problem of multilayer thin films.

2 Theory of the Iterative Four Terminal Networks and its Application to the Problem of Alternating Layers

Suppose p identical four terminal networks with no electromotive force within the circuits are connected in cascade in the same direction as shown in Fig. 2.

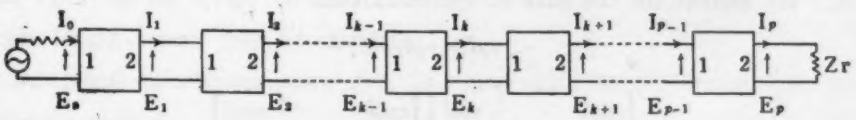

Fig. 2.

A repeated circuit of four terminal networks

The voltage E_k and current I_k at the k-th junction are as follows[6]:

$$\begin{cases} E_k = H_1 e^{-kv} + H_2 e^{kv}, \\ I_k = (H_1/U_1)e^{-kv} - (H_2/U_2)e^{kv}. \end{cases} \tag{8}$$

Where

$$v = \ln[\{(A+D) + \sqrt{(A+D)^2 - 4}\}/2], \tag{9}$$

and

$$\begin{cases} U_1 = \{\sqrt{(A+D)^2 - 4} + (A-D)\}/2C, \\ U_2 = \{\sqrt{(A+D)^2 - 4} - (A-D)\}/2C. \end{cases} \tag{10}$$

Two quantities H_1 and H_2 are determined from the conditions of the sending and the receiving ends.

Now we will consider alternating layers having a structure such as shown in Fig. 3, that is, n_1 and n_2 layers arranged alternately side by side.

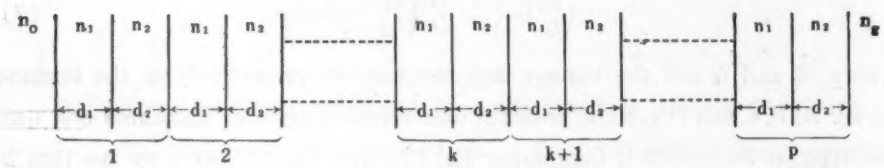

Fig. 3.

The schematic diagram of alternating layers

We may consider the whole structure to be composed of p iterative sets, each of which consists of two layers n_1 and n_2 as indicated in the lower part of Fig. 3. Then we may compare the alternating layers in Fig. 3 with the iterative networks in Fig. 2, an $(n_1 n_2)$-layer corresponding to a unit four terminal network.

The constants for the $(n_1 n_2)$-layer, corresponding to the four terminal constants, may easily be found by multiplying the matrices of the individual layers.

We assume for the sake of simplicity that

$$v_1 d_1 = v_2 d_2 = \delta;$$

$$\begin{pmatrix} \cos\delta & \frac{i}{w_1}\sin\delta \\ iw_1\sin\delta & \cos\delta \end{pmatrix} \begin{pmatrix} \cos\delta & \frac{i}{w_2}\sin\delta \\ iw_2\sin\delta & \cos\delta \end{pmatrix}$$

6) E. A. Guillemin: "Communication Networks." Vol. II. (John Wiley and Sons, 1935), pp. 161-166.

$$= \begin{pmatrix} \cos^2\delta - \frac{w_2}{w_1}\sin^2\delta & i\left(\frac{1}{w_1}+\frac{1}{w_2}\right)\sin\delta\cos\delta \\ i(w_1+w_2)\sin\delta\cos\delta & \cos^2\delta - \frac{w_1}{w_2}\sin^2\delta \end{pmatrix} \tag{11}$$

That

$$\begin{cases} A=\cos^2\delta-\frac{w_2}{w_1}\sin^2\delta, & B=i\left(\frac{1}{w_1}+\frac{1}{w_2}\right)\sin\delta\cos\delta, \\ C=i(w_1+w_2)\sin\delta\cos\delta, & D=\cos^2\delta-\frac{w_1}{w_2}\sin^2\delta. \end{cases} \tag{11}'$$

Substituting Eqs. (11)′ into Eqs. (9) and (10), we may found ν, U_1 and U_2. From the condition that the refractive index of the left hand medium is n_0, we have $g_0=w_0f_0$, and then

$$\begin{cases} H_1=\{U_1(1+w_0U_2)\}f_0/(U_1+U_2), \\ H_2=\{U_2(1-w_0U_1)\}f_0/(U_1+U_2). \end{cases} \tag{12}$$

Putting Eqs. (12) into Eqs. (8), we find that

$$\begin{cases} f_k=f_0\{U_1(1+w_0U_2)e^{-k\nu}+U_2(1-w_0U_1)e^{k\nu}\}/(U_1+U_2), \\ g_k=f_0\{(1+w_0U_2)e^{-k\nu}-(1-w_0U_1)e^{k\nu}\}/(U_1+U_2). \end{cases} \tag{13}$$

Next, since the refractive index of the right hand medium is n_g, the reflectivity R_{2p} of a $2p$-layerd filter may be given as follows:

$$R_{2p}=|(w_gf_p-g_p)/(w_gf_p+g_p)|^2$$

$$=\left|\frac{-2(w_0w_gU_1U_2-1)\sinh p\nu+(w_0-w_g)(U_1+U_2)\cosh p\nu-(w_0+w_g)(U_1-U_2)\sinh p\nu}{-2(w_0w_gU_1U_2+1)\sinh p\nu+(w_0+w_g)(U_1+U_2)\cosh p\nu-(w_0-w_g)(U_1-U_2)\sinh p\nu}\right|^2 \tag{14}$$

3 Discussion on the Formula of Reflectivity

For the sake of simplicity, we consider only the case in which light is incident normally on the surface of a filter. In this case $w_0=n_0$, $w_1=n_1$, $w_2=n_2$ and $\delta=\frac{2\pi}{\lambda}n_1d_1=\frac{2\pi}{\lambda}n_2d_2$ (neglecting the dispersion of each layer). If n_0, n_1, n_2, d_1 and d_2 are given, δ may be determined by λ, and the reflectivity of the light of wave length λ may then be calculated.

Numerical calculations using Eq. (14) can easily be performed with the following procedure:

i) computation of $(A+D)/2=\cosh\nu$.

ii) computation of $\sqrt{(A+D)^2-4}/2=\sinh\nu$.

iii) computation of $\sqrt{(A+D)^2-4}/C=U_1+U_2$,

iv) computation of $(A-D)/C=U_1-U_2$,

v) determination of ν from the result of i) ((ii) is useful as a check for this determination),

vi) multiplication of ν by p, and determination of $\sinh p\nu$ and $\cosh p\nu$,

vii) computation of R_{2p}.

In the numerical calculation, the values of MgF_2 and ZnS were taken for n_1 and n_2, namely $n_1=1.38$ and $n_2=2.38$. The variation of ν, (U_1+U_2) and (U_1-U_2) in the above case are shown in Figs. 4 and 5. In the cases of $r_0=1.0$, $n_g=1.52$ and $p=1, 2, 3$ and 4, the results of calculations for R_{2p} agree perfectly with those previously obtained on Weinstein's method. (Fig. 6).

Further, to discuss the characteristics of Eq. (14), we must examine the behaviour of ν. ν is found from Eq. (9), and is generally complex.

We put

$$\nu=\alpha+i\beta. \tag{15}$$

When $|A+D|<2$

$$\alpha=|\nu|=0,$$

$$\beta=\arg\nu=\tan^{-1}\frac{\sqrt{4-(A+D)^2}}{A+D}, \tag{16}$$

that is ν is purely imaginary.

When $|A+D|>2$

$$\begin{cases}\alpha=|\nu|\\ \beta=\arg\nu=m\pi\end{cases}\quad(m=1, 2,\cdots\cdots) \tag{17}$$

that is ν is complex.

In the case under consideration, the condition $|A+D|\lesseqgtr 2$ is identical with the condition $|\cos\delta|\gtreqless\left|\frac{n_1-n_2}{n_1+n_2}\right|$. This relation is clearly shown in Fig. 4.

Now we will assume the number of layers $2p$ to be very large. In the region where ν is imaginary, since $\sinh(p\nu)=-i\sin(ip\nu)$ and $\cosh(p\nu)=\cos(ip\nu)$, R_{2p} vibrates p times during the time that δ increases from 0 to $\cos^{-1}\left|\frac{n_1-n_2}{n_1+n_2}\right|$, and is small in magnitude. In the region where ν is complex, since $\sinh(p\nu)\fallingdotseq\cosh(p\nu)$, R_{2p} has a value almost equal to unity. When $\delta=\cos^{-1}\left|\frac{n_1-n_2}{n_1+n_2}\right|$, the numerator and the denominator of Eq. (14) are both 0, but if we calculate the limit

ing value of R_{2p} when $\cos\delta$ tends to $\left|\frac{n_1-n_2}{n_1+n_2}\right|$, we may obtain a definite value, and we find that this value approaches unity as p increases to infinity.

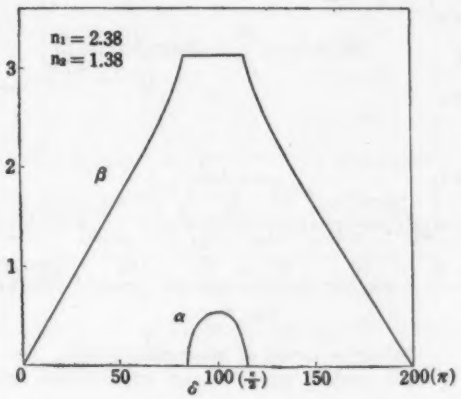

Fig. 4.

Variation of $\nu=\alpha+\beta i$

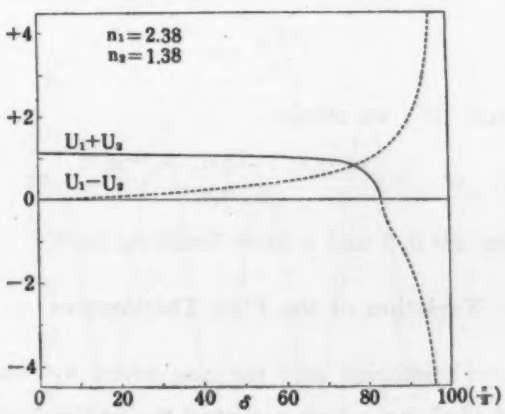

Fig. 5.

Variation of (U_1+U_2) and (U_1-U_2)

—— real

..... imaginary

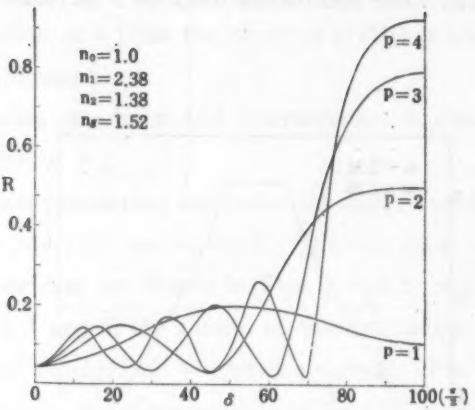

Fig. 6.

Reflection curves of alternating layers.

Further, we will assume that $n_g=n_0$, and the second term of the numerator and the third term of the denominator of Eq. (14) will vanish:

$$R_{2p}=\left|\frac{(n_0U_1-1)(n_0U_2+1)\sinh p\nu}{(n_0^2U_1U_2+1)\sinh p\nu+n_0(U_1+U_2)\cosh p\nu}\right|^2. \tag{18}$$

The envelope Φ of $R_2'_p$ will be found from the equation

$$\frac{\partial R'_{2p}}{\partial p}=0 \tag{19}$$

Solving Eq. (18) and (19), we obtain

$$\Phi=0, \quad \text{or} \quad =\frac{(n_0^2-n_1n_2)^2+n_0^2(n_1-n_2)^2\tan^2\delta}{(n_0^2+n_1n_2)^2} \quad \text{or} \quad =1. \tag{20}$$

The three envelopes are 0, 1 and a curve involving $\tan^2\delta$.

4 Variation of the Film Thicknesses

So far we have considered only the case where $n_1d_1=n_2d_2$. If this is not the case, that is, if $(2\pi/\lambda)n_1d_1=\delta_1$ is not equal to $(2\pi/\lambda)n_2d_2=\delta_2$, the reflectivity curve will be different from the one discussed above. In order to consider this former case, we must return to Eq. (11).

The multiplication of the matrices results in

$$A=\cos\delta_1\cos\delta_2-\frac{n_2}{n_1}\sin\delta_1\sin\delta_2,$$

$$B=i\left(\frac{1}{n_2}\cos\delta_1\sin\delta_2+\frac{1}{n_1}\cos\delta_2\sin\delta_1\right),\qquad(21)$$

$$C=i(n_1\sin\delta_1\cos\delta_2+n_2\cos\delta_1\sin\delta_2),$$

$$D=\cos\delta_1\cos\delta_2-\frac{n_1}{n_2}\sin\delta_1\sin\delta_2.$$

We put,

$$\delta_1+\delta_2=\Delta,\qquad\qquad \delta_1-\delta_2=\varepsilon$$

$$A+D=\frac{1}{2n_1n_2}\{(n_1+n_2)^2\cos\Delta-(n_1-n_2)^2\cos\varepsilon\}.\qquad(22)$$

According to the present theory, in the region where

$$\{(A+D)^2-4\}>0.$$

ν is complex, and the reflectivity has a large value, Fig. 7 shows the $\{(A+D)^2-4\}$ curve for three cases, (I) is the curve for $\varepsilon=0$, that is $\delta_1=\delta_2$, and has a positive value in the vicinity of $\Delta=\pi, 3\pi, 5\pi,\ldots\ldots$. (II) is for $\varepsilon=\Delta$, that is $\delta_2=0$, and does not have a positive value, (III) is for $0<\varepsilon<\Delta$, and has a positive value in the vicinity of each π position but in ranges narrower than in the case of curve (I). However, the curve for $\Delta=m\varepsilon$ ($m=2, 3,\ldots\ldots$) dose not have a positive value in the region near $\Delta=2km\pi$ ($k=1, 2, 3,\ldots\ldots$).

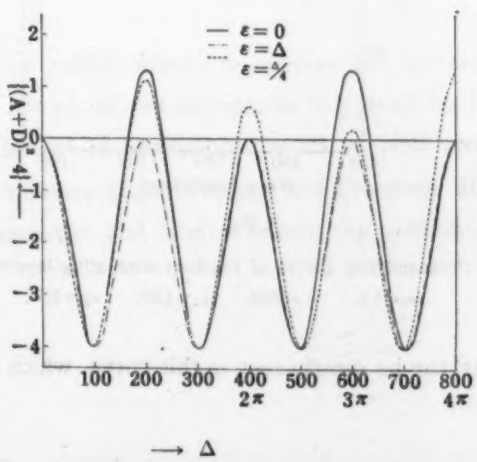

Fig. 7.

From the above discussion it is safe to conclude that, (1) when $\delta_1=\delta_2$, large maxima appear in the reflectivity curve at the positions $\Delta=\pi$, 3π, 5π,..... (2) However, when $\delta_1 \neq \delta_2$ large maxima in the reflectivity curve appear at the positions $\Delta=\pi$, 2π, 3π,....., their widths being somewhat narrower.

5 Experiments to Substantiate the Theory

Banning[7] already published the reflection curves of filters of this type. But in her curve the small maxima expected from our theory were not present.

Filters having seven layers of zinc blend and seven layers of cryolite on glass were carefully made by vacuum evaporation, and the transmission curves were plotted by a G. E. Recording Spectrophotometer (Fig. 8). The slit width was 10 mμ.

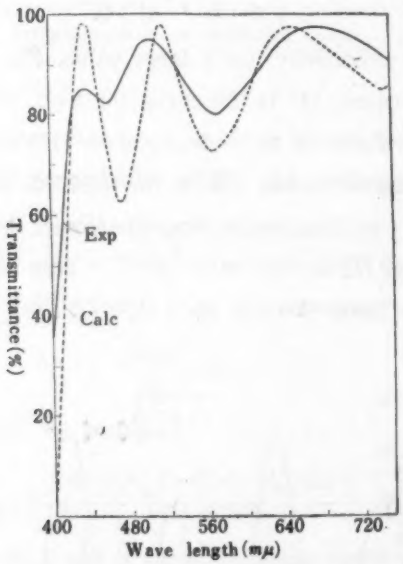

Fig. 8.

Transmission curves of fourteen alternating layers.
$n_0=1.0$, $n_1=2.38$, $n_2=1.38$, $ng=1.52$,

Small maxima can be clearly seen in this curve which agree very well with the theory.

7) M. Banning: J. O. S. A. 38, 792 (1947);

6 Interpretation of the Reflection Spectrum from the Crystals of Chlorate of Potash according to the Present Theory

The iridescent color of crystals of chlorate of potash has been observed by many authors[8]. The spectrum of the reflected light from the crystal was found to consist of very narrow bands. The cause of this spectrum was explained by the existence of a periodic twinning within the crystal. This crystal can therefore be considered an alternating layer type interference filter with a large number of layers. From this point of view, the width and the wave length of the band could be estimated by utilizing the present theory.

The refractive indices of chlorate of potash crystals are[9] $n_\alpha=1.440$, $n_\beta=1.515$, $n_\gamma=1.525$. If we assume that the twinning occurs in such manner that the n_β and n_γ layers appear alternately, the width of the band can be estimated to be 25 Å in the first order reflection band near the D-line, and to be 8 Å in the second order band. This value differs somewhat from the experimental data of 10～12 Å obtained by Wood[10]

The ratio of the wave lengths of the reflection bands of 1st, 2nd,…… order must be $1:1/3:1/5:\cdots\cdots$ for equal thickness, according to the present theory, but in the experiment this ratio was $1:1/2:1/3\cdots\cdots$. This descrepancy can be well explained by the discussion in (4) on the unequality of thickness in the component layers.

In conclusion the author wishes to express his appreciation of the encouragement and kind advice offered throughout this work by Professor Kwan'ichi Asagoe and to Dr. Robert B. Muchmore for his valuable comments. The author also is grateful to Professor Yoshio Fujioka and Professor Hiroshi Kubota who kindly read the manuscript and offered helpful suggestions.

8) Lord Rayleigh Jr.: Proc. Roy. Soc A, **102**, 688 (1923). R. W. Wood: "Physical Optics" .3rd Ed. (Macmillan Book Co., New York) pp. 198- 202. 9) International Critical Tables; 10) R. W. Wood: loc. cit..

A Hard and Efficient Reflection-Reducing Coating

Tsukasa SAWAKI and Hiroshi KUBOTA

Institute of Industrial Science, Tokyo University, Chiba-City.

(Received Jan. 15, 1953)1)

Synopsis……

Double layer reflection-reducing coating which is quite suitable for the instruments used with monochromatic or nearly monochromatic light is discussed. To apply this layer to the instruments used with white light such as bioculars, camera lenses etc., the values of the luminaence of the reflected light were calculated. Results showed that it is possible to get good layer for such a purpose if the thickness of the layers are slightly alterd. Results of the experiments are compared with the calculated values. They show a good agreement.

1 Introduction

In reflection-reducing layers coated on glass surface, the refractive index of the layer must be equal to the square root of that of the glass in order to render the reflection zero for a certain wavelength. The refiectivity of such a layer is very low throughout the visible range as shown by the line (A) in Fig. 1. No

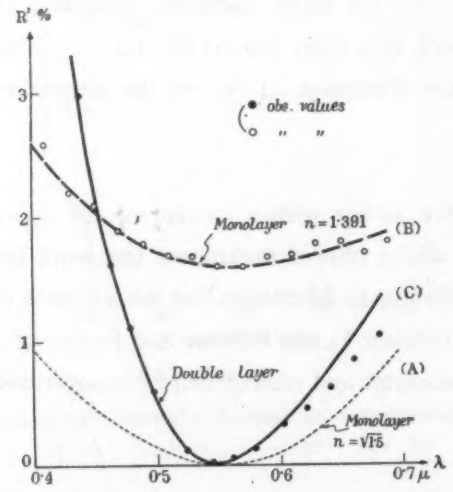

Fig. 1. Spectral reflectivity curves of various reflection-reducing coatings.

substance actually in existence however posses a refractive index so low as to satisfy this condition. Curve (B) in Fig. 1 is the spectral reflectivity of a hard

coated MgF_2 layer, whose refractive index is the lowest among practically useful materials. The minimum reflectivity of this layer is about 1.6 %, which means that the refractive index n of the layer is about 1.39, taking $n_g=1.50$, the index of refraction of the glass. This is far above the ideal value $\sqrt{1.50}$. We must therefore conclude that there is little hope of obtaining an efficient and durable reflection-reducing layer with the use of monolayers, and this leads us to the consideration of the multiple, or at least double, layers. For this reason, we have surveyed for the possibilities of a combination of commonly used substances such as MgF_2 ($n=1.40$ when coated hard) and ZnS ($n=2.20$).

2 The Double Layers.

The reflectivity in amplitude of a double layer when the light is perpendicularly incident upon it, may be given as follows:

$$R=\frac{r_2[1+r_1r_0\exp(-i\delta_1)]+[r_1+r_0\exp(-i\delta_1)]\exp(-i\delta_2)}{1+r_1r_0\exp(-i\delta_1)+r_2[r_1+r_0\exp(-i\delta_1)]\exp(-i\delta_2)}.$$

where r_j represents the reflectivity in amplitude at the boundary of each layer as shown in Fig. 2, and $\delta_j=4\pi(n_jd_j)/\lambda$, (n_jd_j) being the optical thickness of each

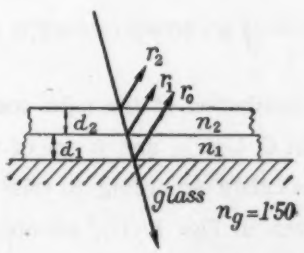

Fig. 2. Double layer.

layer and λ the wavelength of the light. We will first consider the condition for zero-reflection for a given wavelength λ_0. This is obtained by giving the value zero to the real and imaginary parts of the above equation, and we thu shave the following solutions[1] for $n_g=1.50$, $n_1=2.20$ and $n_2=1.40$:

$$\tan(\delta_1/2)=\pm 0.419, \qquad \tan(\delta_2/2)=\pm 1.935. \tag{1}$$

From this we are given two solutions, that is:

1) P. King and L. B. Lockhart. Jour. Opt. Soc. Am., 36 (1946) 513.

$$\text{(i)}\begin{cases}(n_1d_1)=0.063\ \lambda_0,\\(n_2d_2)=0.326\ \lambda_0,\end{cases}\qquad\text{(ii)}\begin{cases}(n_1d_1)=0.437\ \lambda_0,\\(n_2d_2)=0.174\ \lambda_0.\end{cases}\tag{2}$$

If we assume the wavelength, whose reflection intensity is made zero, to be $\lambda_0=546\ \mathrm{m}\mu$, the optical thicknesses of the layer become as follows:

$$\text{(i)}\begin{cases}(n_1d_1)=\ 34.5\ \mathrm{m}\mu,\\(n_2d_2)=178\ \mathrm{m}\mu,\end{cases}\qquad\text{(ii)}\begin{cases}(n_1d_1)=240\ \mathrm{m}\mu,\\(n_2d_2)=\ 95\ \mathrm{m}\mu,\end{cases}$$

The spectral reflectivities of these layers are given in Fig. 1 by the line (C) and in Fig. 5. The first solution is the same as that already discussed briefly by H. Osterberg*[2]. These layers are quite suitable for instruments used with monochromatic or nearly monochromatic light.

3 Luminance of the Reflected Light

Now, for many optical instruments used mostly with white light, we have to consider effect of the layer in the visible region as a whole. We shall first consider the solution (i) of Eq. (2). To compare the effect for white light, we must calculate the luminance of the reflected light, given as the Y-value of the tristimulus values of C. I. E. thus,

$$\int E\cdot R^2\cdot\bar{y}\cdot d\lambda=Y,$$

Where E is the energy distribution of the light source (in this paper we shall used the "C-light source of C. I. E."), and $\bar{y}$ one of the tristimulus values of the spectrum color. If we calculate according to this formula, the Y-value of the MgF_2 layer ($n=1.39$) given in Fig. 1 (B), we obtain the figure 1.65 %, which becomes 0.30 % in the case of the double layer given in Fig. 1 (C). This shows that the latter is sufficiently effective even for white light.

Now, we might ask: could there be any other layer even more effective? To find the answer to this question we performed calculations on various combinations of thicknesses of the first and second layers. The result is shown in Fig. 3, which curve is drawn with (n_1d_1) as parameter and (n_2d_2) as abscissa. We may see from this figure that the minimum value takes place when $(n_2d_2)\fallingdotseq180$

* If we replace ZnS by TiO_2 ($n=2.50$), we have $(n_1d_1)=0.047\lambda_0$, $(n_2d_2)=0.333\ \lambda_0$. The reflectivity of this layer is slightly smaller than in case of ZnS.

2) H. Osterberg and W. H. Kashdan. Jour. Opt. Soc. Am., **42** 291 (A) (1952).

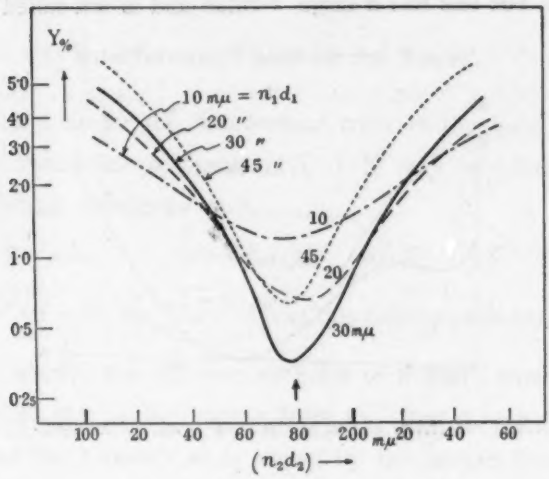

Fig. 3. Luminance of reflection-reducing double layers.

mμ, irrespectively of the value of (n_1d_1). Further, if we plot the Y-values of $(n_2d_2)=180$ mμ, taking (n_1d_1) as abscissa (shown marked ○ in Fig. 4), Y assumes a minimum value when $(n_1d_1)=30\sim35$ mμ. This is roughly equivalent to the solution (i) of Eq. (2) with the value of λ_0 at about 550 mμ, the wavelength at which $\bar{y}$ is maximum.

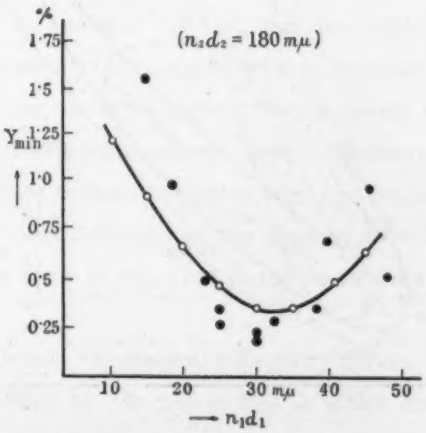

Fig. 4. Luminance of reflection-reducing double layers.

If we take the solution (ii) of Eq. (2), we obtain the spectral reflectivity shown in Fig. 5, but this has a large Y-value and is not suited for instruments

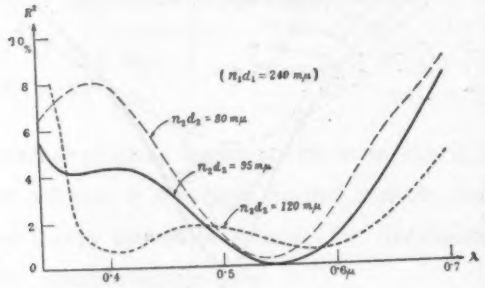

Fig. 5. Spectral reflectivity curves of the layer given by solution (ii) of Eq. (2).

used with white light. If we vary (n_2d_2), keeping (n_1d_1) constant at 240 mμ, the curve changes form assuming the shape shown in the figure, and when $(n_2d_2) =$ 120 mμ, under which condition nearly zero reflectivity is reached at two wavelengths, thus manifesting characteristics of an achromatic reflection-reducing

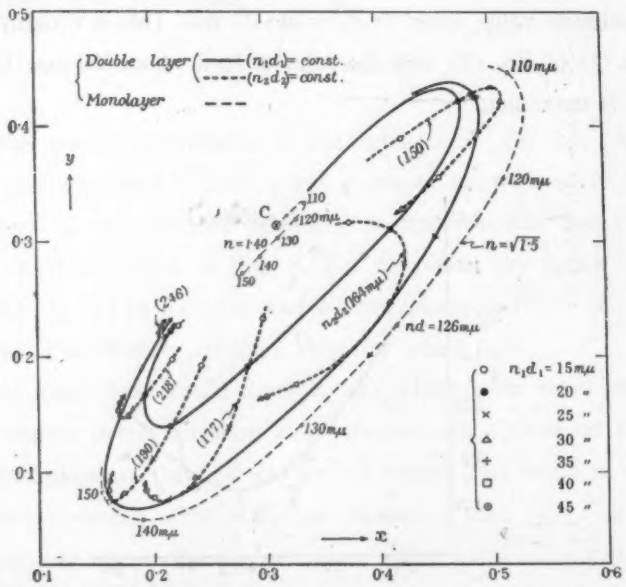

Fig. 6. Interference color of double layers (Thick lines), with that of monolayers drawn in with thin lines for reference.

layers[3]. However, this layer still has the fatal drawback of a large Y-value, so we will not consider this solution further.

4 Interference Color of the Layer

Next, we shall consider the interference color of the light reflected from these layers. The tristimulus cordinates of C. I. E. may be calculated from the values of their spectral reflectivity thus,

$$x=X/S, \qquad y=Y/S, \qquad S=X+Y+Z,$$

where $X=\int E \cdot R^2 \cdot \bar{x} \cdot d\lambda$, etc. The result of this calculation is shown in Fig. 6.

As has been shown, the interference color of a MgF_2 monolayer with refractive index $n=1.40$, that is, far remote from $\sqrt{n_g}$, has a very poor purity, its curve passing near the C-point[4] as is shown by the broken line in Fig. 6. On the other hand, the purity of the interference color of the double layer increase with the thickness of the first layer (as shown by the thick dotted lines in the figure), and reach maximum when $(n_1d_1)=30\sim35$ mμ. In such case, the loci of the color nearly coincide with the outermost thin broken line in the same figure representing the interference color of an ideal layer, whose $n=\sqrt{n_g}$. With a further increase of (n_1d_1), the purity of color decreases again. We may notice from the same figure fhat the interference color of all the layers giving minimum Y, that is, layers whose $(n_2d_2)=180$ mμ for any (n_1d_1), have roughly the same dominant wavelength. This indicates that after the first layer is coated by a suitable methode (e. g. by utilizing the fact that the thickness of the layer is nearly inversely proportional to the square of the distance between the glass and the evaporating source, or by weighing the material to be evaporated), it is only necessary in coating the second layer to observe the interference color of this layer in order to know when to stop the evaporation, and furthermore, judgement of the final thickness of the layer by its color is much fascilitated by the fact that the color in this case is far purer than in the case of the monolayer.

Y-values calculated from the spectral reflectivity curves of the layers coated in such a way are indicated by • marks in Fig. 4, which show good agreement

3) A. Vasicek. Optica Acta. 20 (1951). A. F. Turner. Jour. de Phys. et Radium, 11 444 (1950).
4) H. Kubota. Jour. Opt. Soc. Am., 40 146 (1950).

with the theoretical values given by the full line.

5 Photographically Effective Layer

The most effective reflection-reducing layer for camera lens or for astronomical telescope objectives is not the one which has the lowest Y-value, but the lowest V-value, which V is given by:

$$\int E \cdot R^2 \cdot \bar{v} \cdot d\lambda = V,$$

where $\bar{v}$ is the spectral sensitivity of the photographic plate.

If we take, for example, the $\bar{v}$-values of the Agfa Isochrom, the Ilford Hyperpanchromatic and the Kodak Superpanchromatic plates[5], we see that for the monolayer, $(nd)=116$ mμ gives the minimum V-values (roughly the same for all plates), its coordinates of the interference color being $x=0.5254$ and $y=0.4138$, that is roughly yellow orange. For the double layer, the best result is obtained when the thickness of the second layer is $(n_2d_2)=150$ mμ. If we plot the V-values by taking (n_1d_1) as abscissa, keeping (n_2d_2) constant at 150 mμ, we see that the thickness $(n_1d_1)=25$ mμ gives the lowest V-values. So we may conclude that this layer is the most effective for photographic purposes, the color of which is $x=0.4958$ and $y=0.4339$, that is, roughly yellow orange, same as in the case of the monolayer.

Acknowledgements

The authors wish to express their sincere appreciation for the invaluable help rendered them in this study by Mr. K. Hara of the Shonan Optical Layers Company. It must also be mentioned that the work was financially supported by the grants in aid for fundamental scientific researh administered by the Ministry of Education.

5) A. van Kreveld. Jour. Opt. Soc. Am., **29** 327 (1939).

Odour, as a Problem of Physics

Yoshio FUJIOKA

Institute for Optical Research, Tokyo University of Education

(Received March 6, 1953)

The phenomenon of odour is nothing but the excitation of the olfactory nerves by molecules that smell, just as in the case of vision which is the excitation of the visual nerves by photons or light waves. In the latter case, light waves in the visible region would excite the nerves, while the waves outside this region would have no effect on them. Does anything similar exist in the domain of odour? In other words, are there certain regions in the energy levels of molecules, corresponding to the visible region of the spectrum of light to which the olfactory nerves are peculiarly sensitive? This is the problem treated in this paper. The writer assumed the existence of a "smell region", in line with the above analogy, and made an investigation of the electronic and the vibrational energies of the molecules belonging to this region. The conclusion is that the sensible range of the molecular electronic energy is that corresponding to the spectrum of 2,000~10,000 A, while that of the vibrational energy would seem to be divided into two regions namely 600~700 cm^{-1} and 1,600~1,800 cm^{-1}.

1 Introduction

Obviously optics is a science concerned with natural phenomena related to the visual sensation, and according to it the varieties of colors are explained as differences in the wave-length of the light waves. Analogously, acoustics is a science related to the aural sensation, in which it is explained that the tone of the sound is related to the wave-length of the sound waves. However, the sciences of optics and acoustics are not concerned with the investigation of visual or aural sensations themselves. Such investigations are the problems of physiology. Workers in optics and acoustics do not investigate the sensations; they study natural phenmena related to them, though eventually development in these sciences could possibly contribute also to the study of the sensations.

Now, although we have the sciences of optics and acoustics as the branches devoted to phenomena related to the visual and aural sensations, what can we say of the other senses? The sense of touch is broadly speaking the effect of pressure, and we will not consider it further for the present. So we are left with the senses of taste and smell. These two senses are rather similar in their mode of stimulation, and the more primitive animals seem to have no power to distinguish between the two. Although the sense of taste would appear to be more complicated, it is already an object of study to some extent in the scientific field

of chemistry. It would seem to the writer that odour is the only phenomenon which has scarecely received scientific consideration so far. The present paper limits itself to a discussion of the sense of odour, but the essence of the argument might also be applied to the problem of taste.

What do we know about odour? Odour has not even been adequately classified. This is a good contrast to the case of the classification of light, since the theory of the three colors was known to us even before the development of optics. It is true that theories analogous to that of the three colors have been presented in the domain of odour, but it has not yet been generally accepted. Besides this classification, we have scarecely any scientific knowledge about odour.

In optics, we arrange the colors along a spectrum according to the wavelength. The relation between color sensation and optics has its basis on the fact first, that we are able to distinguish each monochromatic color by corresponding sensations from which we distinguish the different colors of the spectrum, and secondly, that this same spectrum is the object of study in optics. A similar relation holds true in the case of the sense of hearing and the science of acoustics. However, the situation is quite different when it comes to odour. We can neither classify odours nor arrange them on a spectrum or a scale. We do not know the reason for this difficulty we meet in attempting to classify the smells ; perhaps it is that odours cannot be arranged along a one-dimensional scale but must be considered in relation to a multi-dimensional system of some sort. The writer however would prefer to attribute the true reason for the difficulty to the fact that no such thing as a monochromatic smell exists; smells seem to be intrinsically polychromatic and it should be impossible to produce a monochromatic smell artificially.

Under these circumstances it would seem very difficult to attempt to analyse polychromatic smells into its components in order to arrange them on a scale. The writer is not choosing this method of approach ; the present study is a quest for what would be the natural phenomenon corresponding to the sensation of smell. We might compare it to the case where we would be searching for the visible wave-length range of the electromagnetic wave without knowing the spectral arrangement of the color.

Before proceeding further, there is one thing to be remarked. The smells of some chemical substances such as Br, HCl, NO and NH_3 have a destructive character, and in such cases the sensation may be attributed to the effect of this character on the nerve cells. The effect of such destructive gases should be treated as a problem of a different category.

2 Is Odour Related to the Energy of the Molecule?

It is clear that the sensation of smell is caused by the stimulation of the olfactory nerves by molecules that are odorous; now the problem is whether the stimulating action is the effect of single molecules or that of molecules acting as a group. We are extremely sensitive to odour and we may smell some substances even in extremely dilute concentrations. This fact would suggest that the sensation of smell is the effect of single molecules. Then we must assume the existence of an interaction between the cells of the olfactory nerves and odorous molecules, accompanying the exchange of energy between one and the other. There are two forms of molecular energy kinetic and potential, but it is very improbable kinetic energy should have any significance in this case, because the temperature of molecules coming into contact with the surface of the nerves cells should generally have approached to body temperature.

Thus it should be concluded that it is the potential energy of the smelling molecules that is exchanged with the cells. Of course it is not an effect of a single collision between two molecules but interaction of a very complicated character, perhaps comparable in its complexity to that of the exchange of energy between photons and the visual nerves when light hits the retina of the eye. But in the latter case, however complicated the mechanism may be, the effect of the photons upon the nerves is determined, and thus subject to classification and arrangement simply according to their energy magnitude or their wave-lengths. Following an analogous consideration, we may ask whether or not it is possible to classify and arrange the effect of smelling molecules upon the olfactory nerves by the magnitude of their energy.

As forms of molecular energy, there are known to us the electronic, vibrational and rotational. The electronic energy may be experimentally observed by the ultraviolet absorption spectrum, while the vibrational and rotational

energies may be measured from the infrared absorption spectrum and the Raman effect. We will proceed to investigate first in the electronic and then in the vibrational energies of the molecules.

We must of course further carefully examine whether or not there are other factors which influence the odour, but we are first treating the problem only from the standpoint of the energy levels of molecules.

3 Is Electronic Energy Related to the Odour? ——"Electronic Smell Region".

When we consider the correlation between odour and the electronic energy of molecules, one attention is drawn to the difference between aromatic and alcoholic compounds. Aromatic compounds, or benzene derivatives, characterized by their strong odour have marked absorption spectra below 2,600 A, while alcoholic compounds, which are devoid of strong smells hardly have any absorption spectra in the visible and the ultraviolet regions. This difference suggests the existence of a relationship between odour and the electronic energy of molecules.

To treat the problem in general, we first direct our attention to gaseous substances which have no smell at all. Among such gases we may count the rare gases He, Ne, Ar and the common gases H_2, O_2, N_2, CO_2 etc.. These gases have no absorption spectrum in the visible and ultraviolet region; their absorption lines are situated below 1,800 A and above 10,000 A. From this fact we assume the following hypothesis:

"Only differences of electronic energy of molecules between 1,800 A and 10,000 A are effective for the stimulation of the olfactory nerves"

These limiting values determining the sensible region are subject to further study and modification, but it may be qualitatively stated that the electronic energy differences corresponding to wave-length belonging to a certain region is related to the odour. We will call this region the "Smell Region" or "Electronic Smell Region".

In the case of light waves, we know the existence of the visible region: light with a wave-length either below or above this region is not sensible to the visual nerves. For the sound, we have the audible region which determines our range of hearing. Now would there not be a similar range of molecular energy

related to the sense of smell? From the above reason, we assume that this range is that corresponding to 1,800 A~10,000 A.

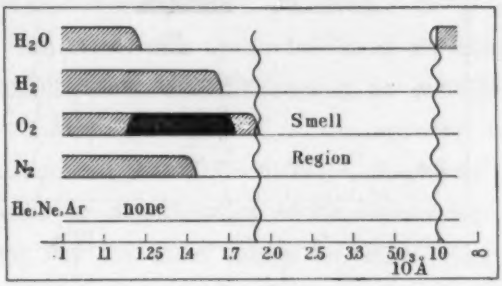

Fig. 1.

In Fig. 1, we show the positions of the absorption spectrum of non-smelling gases and the position of the smell region. For the abscissa is taken the wave-length, in the scale of A.

In this and the following figures, the parts indicated by oblique lines show the positions of band spectra, and black parts show the positions of continuous spectra.

We determined the position of the smell region from the figures pertaining to non smelling substances. The next problem is to investigate whether or not the positions of the absorption spectra of smelling substances always lie within this region. It is of course impossible to investigate all and every organic substance. However, so far as the writer has been able to verify all substances known to have a smell seem to have absorption spectra in this region. In Figs. 2 and 3 we show the positions of the absorption spectra of some simple and well

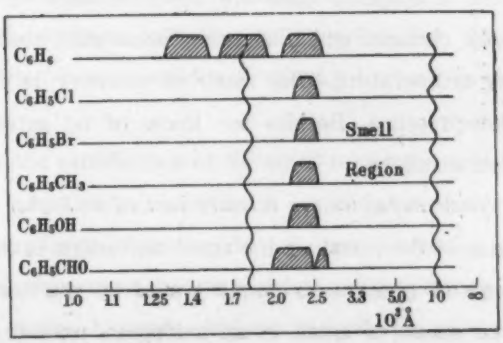

Fig. 2.

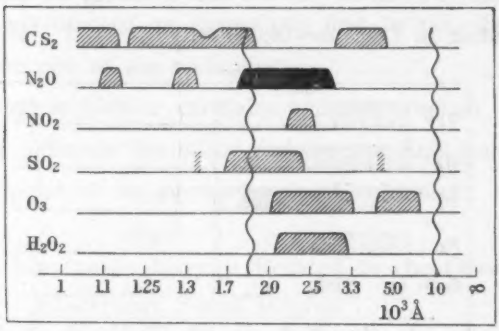

Fig. 3.

known smelling substances.

4 Some Remarks on the Smell Region Hypothesis

a) Non monochromatic character of odour according to the smell region hypothesis.

According to the smell region hypothesis, it should be expected that the position of the absorption spectrum would determine the character of the odour, just as with the color of light, which is characterized by its wave-length. However, the actual fact is that all absorption spectra of molecules in the electric smell region have naturally complicated patterns having vibrational and rotational structures. This means that according to our smell region hypothesis all smells are polychromatic. If we are to look for monochromatic odour, we must find monochromatic absorption lines.

Monochromatic absorption lines are observed only in monoatomic gases. Mercury is the only element which shows monoatomic absorption in the smell region at ordinary temperature. The smell of mercury is very weak probably because of the low-pressure. Besides we know of no substance which would satisfy the required condition.

b) Whether smell molecules are actually excited to higher electronic levels.

The perception of the visual or the aural sensations is caused by the absorption of the energy of photons or sound waves by the nerves. If we consider the problem of the sense of smell in an analogous manner, the stimulation of the nerves by the energy of the molecules must be the origin of the sensation;

moreover, according to our electronic smell hypothesis, it should be quite appropriate to consider that the odorous molecules exist at higher excited electronic levels and that energy is transferred to the cells.

The problem then is: what is the probability of the existence of molecules at the higher excited electronic levels? Obviously the probability is determined by the factor $e^{-\frac{E}{kT}}$, and if we take T as the ordinary temperature and E as the energy corresponding to 2,000~10,000 A, this factor becomes extremely small. It would hardly be possible that odorous molecules would have their energy levels so high. For the same reason we may reject as improbable the inverse phenomenon, which would imply that molecules of the nerve cells, possessed of a state of electronic excited level molecules, would transfer their energy to the latter molecules. Besides, it is also unbelievable that certain particular molecules in the cells should be functioning differently from the rest, since it must be assumed that the specific function of a cell would be performed by the cell as a whole.

Thus the hypothesis of an electronic smell region, based on the idea of an exchange of energy between molecules, would now appear to be difficult to accept on this simple basis alone.

c) Is the electronic sm ll region hypothesis merely superficial?

As stated above, the electronic smell region hypothesis is rather difficult to accept very simply: possibly this hypothesis expresses merely a superficial relation. Indeed, we know that among the innumerable natural phenomena, some relationships do exist which are purely superficial and have no scientific meaning at all related to the actual mechanism. For instance, whether a substance smells or not seems to have some relation with its boiling point, but this relation between odour and the boiling point would not appear to have any further scientific meaning.

To determine the significance of the smell region hypothesis, especially with a view to proving its validity positively, it would be desirable to know the mechanism of the interaction between the odorous molecules and the olfactory nerves. This mechanism must be very complicated, perhaps comparable in its complexity to the action between photons and the visual nerves, and we have very little knowledge about such phenomena. If we knew the mechanism of these

phenomena, it might be possible to understand our hypothesis as the integrated effect of numerous elementary processes. At the present stage, we have no reason to lay claim on the validity of our hypothesis, but there may be no objection to offer it as a phenomenological hypothesis.

5 Is there a Smell Region in Vibrational Levels?

The smell region hypothesis hitherto discussed presents a difficulty in respect to the extremely high excitation energy levels that would have to be assumed, and the hypothesis might more properly be understood as a phenomenological or indirect relation. To consider a state of more direct excitation of molecules, we must take up cases of energy levels of an order that would lend itself to excitation at ordinary temperatures. Such levels are of course vibrational and rotational, and may be observed either through the infrared absorption or through the Raman effect. In many molecules vibrational lines differ in the two spectra, and we are at a loss to tell which spectrum to refer to. We therefore investigated the tables of absorption lines and Raman lines for nearly all known substances.

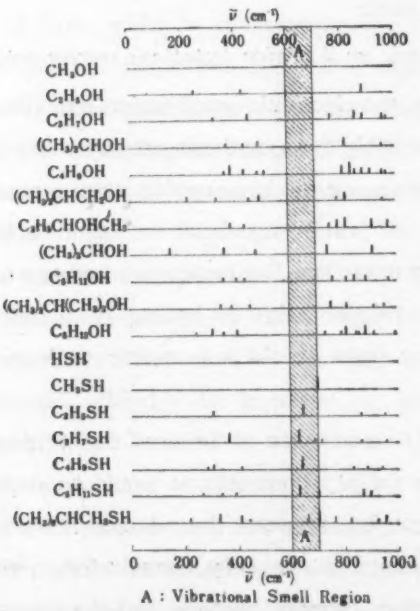

A : Vibrational Smell Region

Fig. 4.

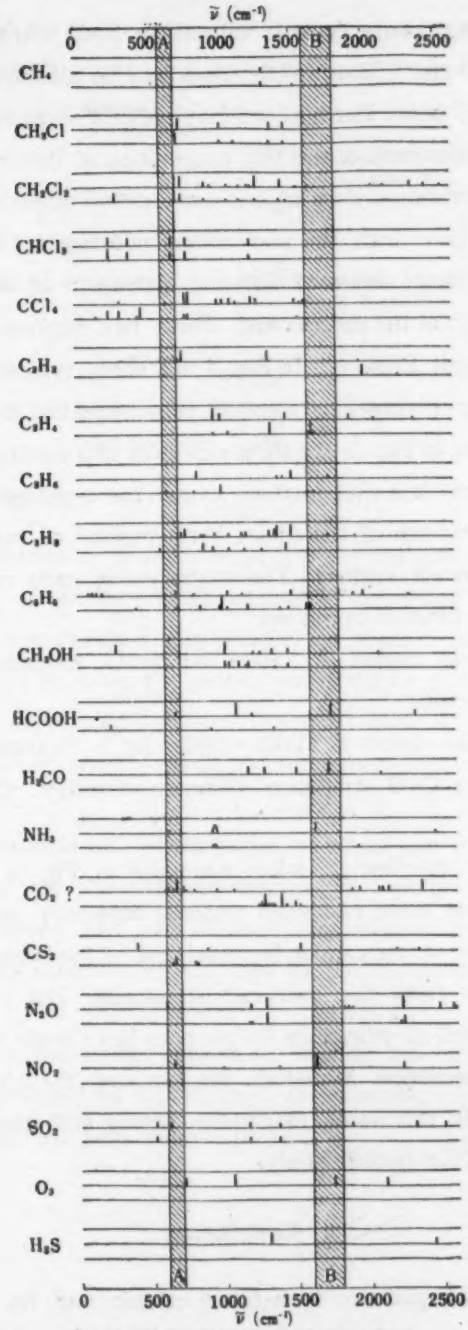

A and B : Vibrational Smell Regions

Fig. 5.

We noticed that many organic substances have vibrational lines between 800 cm^{-1} and 1,600 cm^{-1}. Many of the lines may be attributed to the stretching vibration of the C-C bond. Further, we may notice a difference between smelling and non-smelling substances at the two extremities of this region. The smelling substances have vibrational lines at one end or the other end of this region, which is not the case with the nonsmelling substances. The wave-lengths of these end regions range between 600 and 700 cm^{-1} at the longer end, and 1,600 and 1,800 cm^{-1} at the shorter end. These two regions we will assume to be "Vibrational Smell Regions". In Fig. 4 we show typical examples of these regions, representing nonsmelling alcoholic substances and the case of very badly smelling merceptans. In Fig. 5 we show examples of a variety of substances.

It is to be remarked that in these cases, the smelling substances do not seem to fall in one stretch of the scale; Two regions of rather narrow range may be noted as smell regions. The vibrations in each region are attributed to certain modes of vibration as follows:

Vibrational smell region A (600～700 cm^{-1}) Example: C=S stretching vibrations of mercaptans.

Vibrational smell region B (1,600～1,800 cm^{-1}) Example: C=C stretching vibration of terpene; C=O stretching vibration of esther; CH ↔ CH vibration of benzene.

As is already manifest in some examples in Fig. 5, many exceptional cases are seen against these two smell regions, especially in the case of inorganic substances. The writer cannot be convinced of the existence of these two smell regions merely from the energetic standpoint. But it should be worth noting that the modes of vibrations do seem to have some meaning in connection with the smell sensation. Moreover, the fact that the energies of such vibrations have roughly the same magnitude seems still more noteworthy and might provide the key for further study.

6 Conclusion

The smell region hypothesis, both for electronic and for vibrational levels is undermined by cases of exception, and the writer does not feel brave enough to strongly insist on its correctness. Often he would be stuck when

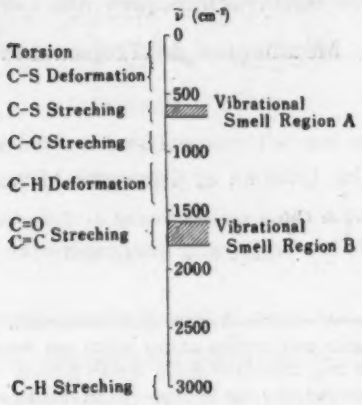

Fig. 6.

queried on some particular problem regarding the phenomenon of smell, because of his entire lack of the knowledge on organic chemistry and physiology.

Our present hypothesis might possibly be entirely fantastic. But were the argument proven to be false, the writer would still be quite satisfied if the present paper should provide an occasion for the attention of scientists to be called on the phenomenon of smell, which has scarcely heretofore become the object of physics.

It is very desirable that investigation be made into the interaction between odorous molecules and the olfactory nerves, as well as that between photons and the visual nerves. The rise of such physiological investigations would be received with immeasuarable gratification by the physicists.

In conclusion the writer wishes to express his hearty gratitude for the unsparing efforts offered by Dr. Ryumyo Ito in assistance to this ambitious and somewhat fantastic but very tedious project.

Etudes Spectrochimiques des Complexes Métalliques du Troponoïde[1]

I[2].

Taku UÉMURA et Seinosuké MIYAKAWA

Laboratoire de Chimie minérale, Institut de Technologie de Tokyo

(Reçu le 4 février, 1953)

Troponoïde is a seven membered carbo-cyclic compound. When two oxygen atoms which are connected with two carbon atoms which are respectively occupied by (1) and (2) position of the ring, tropolone group is then formed. An inner molecular complex salt with five membered ring can be prepared in uniting a metal to the tropolone. We present, in this paper, the absorption spectra of monovalent, divalent, and trivalent metallic complexes of hinokitiol (*m*-isopropyl tropolone). Those are the results of the studies on the relation between the absorption bands of hinokitiol complex and those given by hinokitiol itself.

1 Introduction

T. Nozoé et ses collaborateurs[3] ont déjà publié sur les recherches chimiques des troponoïdes, un groupe des composés à sept chainons constitués par le carbone. Les présents auteurs ont étudié sur des spectres d'absorption des complexes métalliques formés par le troponoïde. Nous allons exposer les résultats obtenus par les recherches spectrochimiques du hinokitiol et ses complexes métalliques. Le hinokitiol (tropolone méta-isopropylique

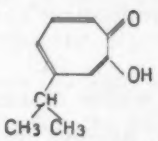

) est un composé à sept chainons constitués par le carbone, et il est facile de substituer par un mét al son hydrogène atomique uni par l'atome d'oxygène. On peut obtenir alorsun complexe interne à cinq chainons comme suit;

1) T. Nozoé et ses collabolateurs ont donné un nom générique "troponoïde" aux dérives des tropones et des tropolones; 2) Exposé fait lors de la Séance spéciale sur les sels complexes de Kantô-shibu (Tokyo) de la Société chimique du Japon, le 13 novembre, (1951);
3) T. Nozoé, Sci. Rep. Tohoku Univ., Ser. I, **34** (1950) 199; Nature, **167** (1951) 1055; Chimie et Industrie chimique (Soc. chim. Japon), **4** (1951) 348.

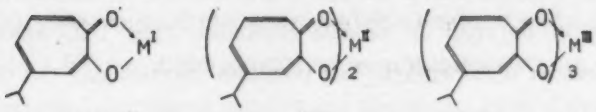

M^{I}, M^{II} et M^{III} représentent relativement l'atome métalliques monovalent, bivalent et trivalent.

2 Procédé expérimental et spectres d'absorption

Nous utilisons des complexes du hinokitiol pour nos recherches en purifiant des combinaisons complexes obtenues par l'addition de solution aqueuse des sels métalliques aux solutions aqueuses du sel de sodium du hinokitiol. H. Iinuma[4] a déjà déterminé les formules chimiques de ces composés étudiés dans le présent mémoire. Nous employons de l'eau comme dissolvant pour le sel de sodium et du méthanol qui peut éviter l'hydrolyse pour les autres.

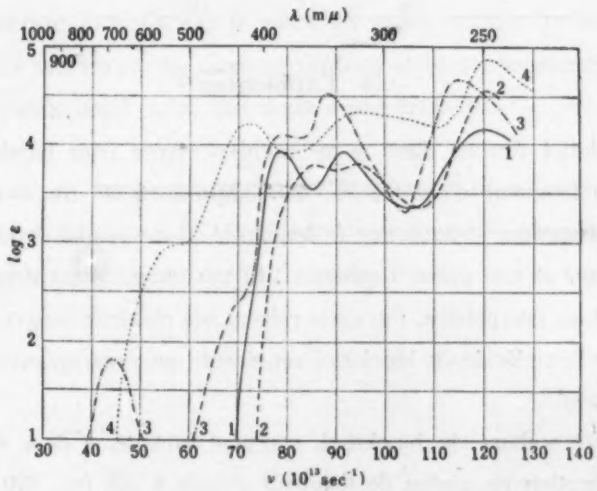

Figure

Absorption des complexes.
1, Hinokitiol; 2, NaHin;
3, CuHin2; 4, FeHin3.

4) H. Iinuma, J. Soc. chim. Japon, **64** (1943) 742; ibid., **64** (1943) 901.

Nous nous sommes servis du spectrophotomètre Spekker construit par Shimazu (Japon), et de celui du modèle Beckman (type DU) américain pour la mesure des spectres d'absorption. Les résultats obtenus par ces deux appareils différents sont bien concordants, et nous pouvons les montrer dans la figure et la table suivantes.

TABLE.

Spectres d'absorption du hinokitiol et ses complexes métalliques
ε=des coefficients d'extinction moléculaire.
λ=longueur d'onde. ν=fréquence.
Hin=hinokitiol.

Composés	λ ($m\mu$)	ν (10^{13}sec^{-1})	log ε
Hinokitiol	383	78.3	3.96
	330	90.9	3.96
	245	122	4.18
Na Hin	356	84.3	3.78
	323	92.9	3.80
	250	120	4.6
Cu Hin_2	680	44.1	1.78
	382	78.6	4.20
	340	88.2	4.52
	260	115	4.73
Fe Hin_3	540	55.6	2.98
	416	72.2	4.22
	314	95.6	4.35
	246	122	4.90

3 Explication

Le hinokitiol dissous dans le méthanol présente trois bandes d'absorption en région de longueur d'onde à 383 mμ, 330 mμ et 245 mμ ayant log$\varepsilon \fallingdotseq 4$. M. Tsuboi[5] a récemment indiqué que le hinokitiol a une grande bande d'absorption à 300—400 mμ, et une autre à environ 240 mμ quand il est dissous par le dissolvant isooctane non polaire. Par cette raison, nos résultats peuvent expliquer que une partie de la molécule du hinokitiol représente un type anionique par la polarité du méthanol.

Le sel de sodium du hinokitiol, composé ionique, a donc également trois bandes d'absorption en région de longueur d'onde à 356 mμ, 320 mμ et 250 mμ.

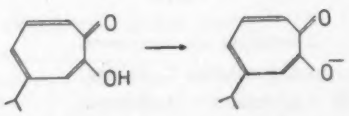

Le sel de cuivre du hinokitiol est différent de celui de sodium en formant

5) M. Tsuboi, Bull. Chem. Soc., Japan, 25 (1952) 369.

un complexe interne par la liaison covalente, et il donne trois bandes d'absorption comme le hinokitiol en région ultraviolette. Ce sel cuivrique a une autre absorption en région visible à 680 mμ qu'on peut trouver aux sels généraux de cuivre.

Le sel ferrique du hinokitiol montre une absorption assez différente de celles du hinokitiol et de ses complexes des métaux monovalents et bivalents. Cette combinaison ferrique donne une dande d'absorption en region visible à 540 mμ et trois bandes au domaine ultraviolet respectivement à 416 mμ, 314 mμ, et 246 mμ. Parmi ces bandes trouvées, celle de 416 mμ est beaucoup plus bathochromique que les bandes correspondantes du hinokitiol et de ses complexes métalliques.

4 Résumé

(1) Nous avons mesuré l'absorption lumineuse des complexes métalliques (Na, Cu, Fe) du hinokitiol en région visible et ultraviolette.

(2) L'absorption lumineuse du hinokitiol dans le méthanol présente trois bandes d'absorption en comportant le type anionique.

(3) Nous pouvons trouver par les complexes de cuivre et de fer une nouvelle bande d'absorption basés sur le métal en région visible. La bande d'absorption ultraviolette formée par le complexe ferrique se trouve en région de longueur d'onde la plus élevée dans celles que nous avons trouvées.

En terminant ce compte-rendu de nos recherches, nous tenons à exprimer nos sincères remerciements à M. T. Nozoé, professeur à l'Université de Tohoku (Sendai), qui a bien voulu nous offrir le hinokitiol employé à nos études actuelles.